Interreg Co-funded by the European Union

Central Baltic Programme

StoPWa

Construction and demolition waste (CDW) characterization study report

Project identification

Project number	CB0100091
Project name	Stormwater purification with construction and demolition waste
Project acronym	StoPWa

Report identification

Reporting period	2
Activity / Deliverable number	D1.2.1
Type of report	Scientific report
Date of report	05.04.2024
Author(s)	Nazila Bolourieh, Teemu Kinnarinen, Arto Pennanen
Organisation(s)	Lut university

LUT University

Table of Contents

Figures

Tables

Acknowledgements

This activity was supported as part of StoPWa, an Interreg Central Baltic Programme 2021-2027 project co-funded by the European Union.

1. Introduction

The aim of the material characterization phase within the StoPWa project is to gather insights into the attributes of construction and demolition waste. These insights are essential for crafting a new filter material dedicated to stormwater purification. Key material characteristics, including particle size distribution, specific surface area, and elemental composition, significantly influence its porous structure and capacity for adsorption. This, in turn, shapes the properties of the final filter product. The following report presents a summary of the characterization findings encompassing all construction and demolition waste streams examined in the Stopwa project.

2. Materials and methods

2.1. Samples

The methodology for selecting construction and demolition waste (CDW) for the characterization study is depicted in Figure 1. To identify the most suitable CDW for the study, discussions and extensive information searches were conducted. Factors such as availability at project locations (Lahti, Tallin, Smiltene), initial particle size, hardness, and asbestos-free status were deemed crucial. Consequently, CDW available within the project locations was prioritized. CDW recycling companies were requested to provide samples with an initial particle size less than 10 mm, and efforts were made to obtain soft (including plastic, insulation materials, textiles, fabrics, etc.) and hard (concrete, brick, cement, ceramic, glass, clay, etc.) samples separately from each location. Subsequently, small random samples were extracted from each batch and sent to an asbestos testing lab to ascertain the absence of asbestos. Samples containing asbestos were excluded from the study, and only asbestos-free wastes were considered further. Additionally, CDW with available information on material properties and statistical data from the industry or literature were deemed particularly relevant for the project.

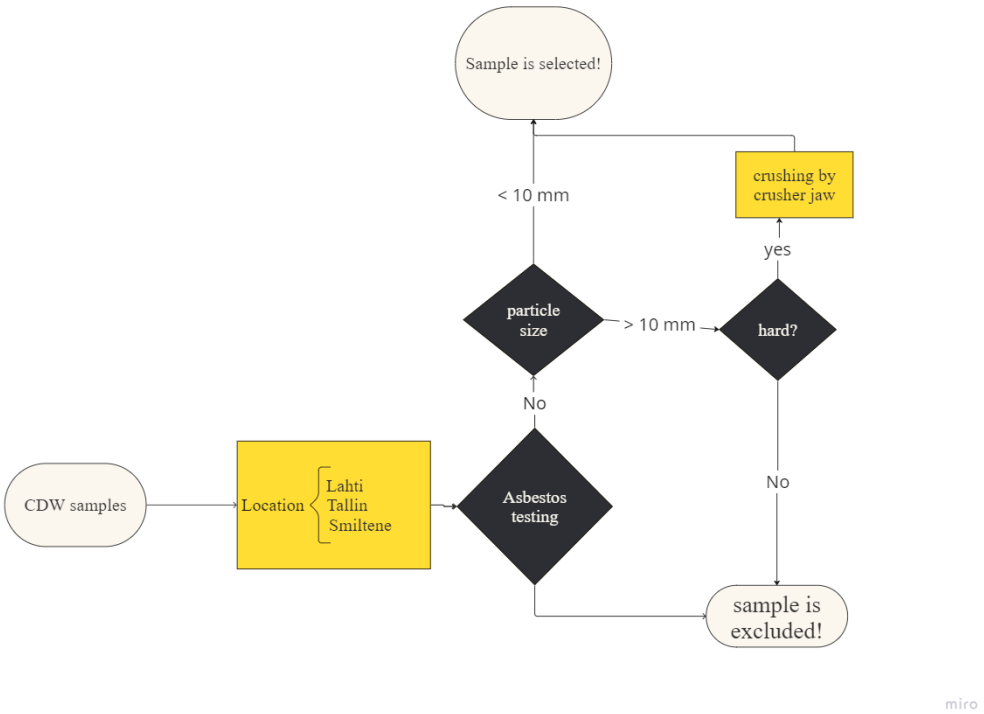

Figure 1. Process of sample selection for characterization study in StoPWa project

The samples which were examined at LUT University during the characterization study of the StoPWa project are detailed in Table 1. Each sample is accompanied by a code assigned for streamlined data management, along with descriptions, original particle size, primary content, treatment methods conducted by recycling companies and LUT University, as well as the particle size and quantity of samples segregated for subsequent characterization and analyses. We selected three samples from recycling companies in the Lahti region, namely Kuusakoski and Salpamaa, from the samples we collected overall. Additionally, our partners in Estonia provided us with several samples, from which we chose two: one representing concrete bricks (hard samples) and the other representing mixed waste comprising insulation materials, wood, and plastic. Furthermore, we acquired a sample from Latvia consisting of a mixture of hard and soft materials, as it was the only sample confirmed to be asbestos-free.

Table 1. Characteristics of chosen construction and demolition waste for study

Sample code	Description	Original particle size (mm)	Main content	Treatment type by original producer	Treatment by LUT researchers	Treated sample particle size (mm)	Treated sample amount (L)
FLSM-0-5	Finland, Lahti, Salpamaa, Mixed waste	0-12	concrete, bricks, porcelain	Screening residue from sorting	Sieved	0-5	5,5
FLSM-2.5-5		0-12				2.5-5	3,5
FLKM-0-5	Finland, Lahti, Kuusakoski, Mixed waste	0-20	wood, foam, soil, plastic, minerals	Screening residue from sorting	Sieved	0-5	4,5
FLKM-2.5-5		0-20				2.5-5	4,5
EACB-0-5	Estonia, ATI group, Concret, Brick	0-25	Concrete, bricks, tiles and ceramics	Crushed, sieved	Sieved, bigger particles crushed to obtain the small particle fraction	0-5	5
EACB-2.5-5		0-25				2.5-5	5
EPM-0-5	Estonia, PTT recycling, Mixed waste	0-5	Mineral components, Wood, Plastic	Crushed CDW, under sieve	Sieved	0-5	4,5
EPM-2.5-5		0-5				2.5-5	4,5
FLSC-0-5	Finland, Lahti, Salpamaa, Concrete brick waste	0-18	concrete (+ bricks etc.) from demolition bricks	material has been cumulated from different operators (during year 2022), the origin of material is not known, then crushing at the plant with an impact crusher in 2022, next, magnetic removal of metals, in the final stage, samples are taken from screening residue <18 mm	Sieved	0-5	5
FLSC-2.5-5		0-18				2.5-5	5
LSZM-0-5	Latvia, Smiltene, Zaao, Mixed waste	0-20	aerated concrete, pluster, tiles, concrete, clay, asphalt, stone mass tiles, insulation materials, brick	Initially mechanical-manual sorting of construction waste at the landfill site, then separating recyclables as far as possible, next, mechanical shredding of the samples	Sieved	0-5	5
LSZM-2.5-5		0-20				2.5-5	2,5

Below, in Figures 2-7, are photographs of the selected samples in their original form. Furthermore, these images depict the samples after separation via sieving, with particle sizes ranging from 0-5 mm as well as 2.5-5 mm.

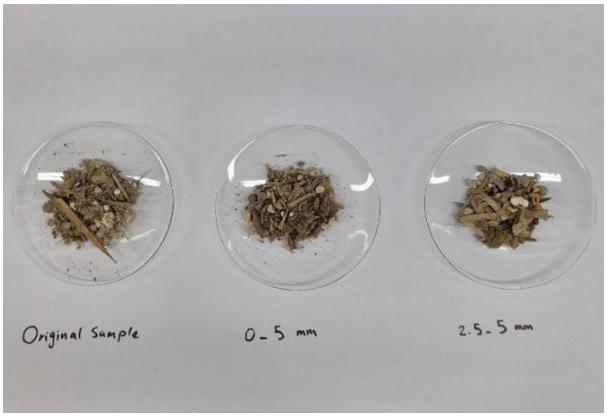

Figure 2. Mixed waste sample from Kuusakoski Oy, Lahti (FLKM)

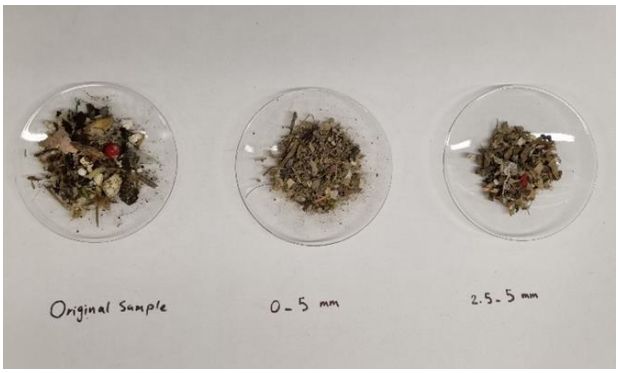

Figure 3. Mixed waste sample from Salpamaa Oy, Lahti, Finland (FLSM)

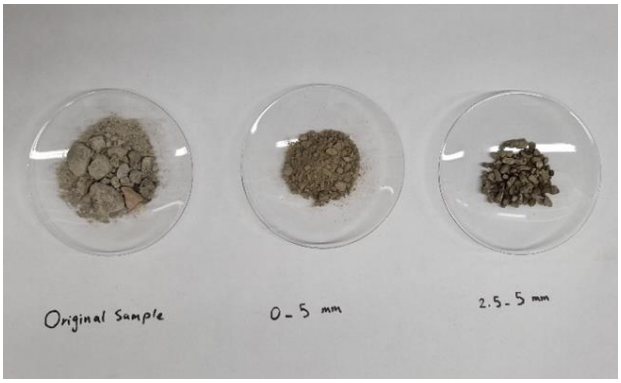

Figure 4. Concrete brick sample from ATI group, Estonia (EACB)

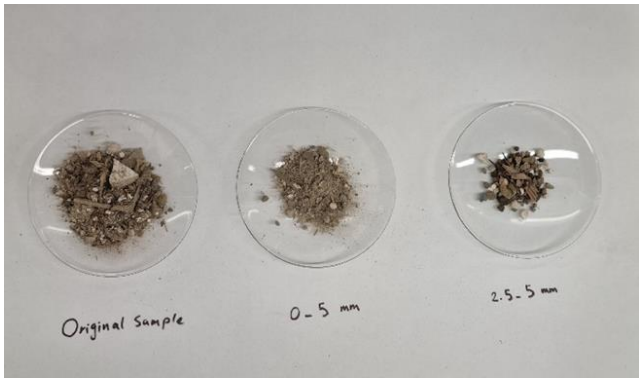

Figure 5. Mixed waste sample from PTT recycling company, Estonia (EPM)

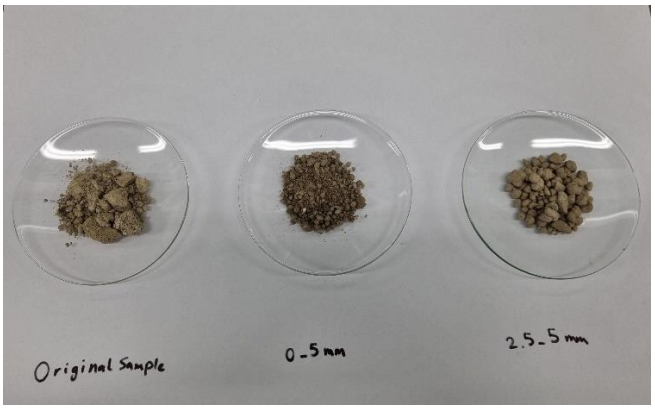

Figure 6. Concrete brick waste sample from Salpamaa Oy, Finland (FLSC)

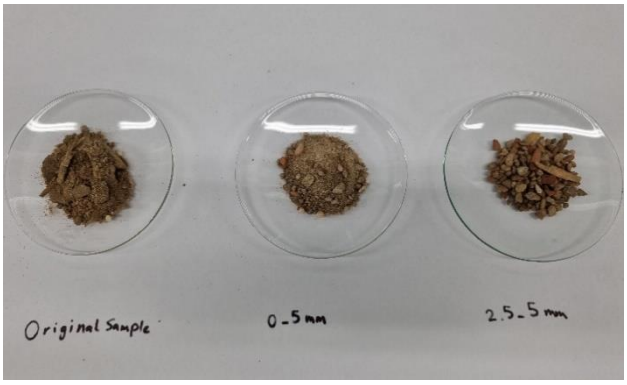

Figure 7. Mixed waste sample from ZAAO company, Latvia (LSZM)

2.2. Construction and demolition waste characterization and analyses methods

Various techniques were employed to characterize the samples, enabling the measurement of particle properties and material composition. Table 2 provides an overview of the characterization and analysis conducted throughout the project. It is noteworthy that not all samples underwent analysis using every available technique. Rather, decisions concerning characterization were made on a case-by-case basis, taking into consideration the chemical composition and overall suitability of each sample for potential filter in stormwater purification.

Table 2. Summary of characterization and analysis of construction and demolition waste

Sample	Fraction	Sample code	SEM-EDS	TGA	BET	PSD (Mastersizer)	PSD (Sieving test)	Morphologi	XRD
Salpamaa mixed waste	0-25µm		N/A	N/A	N/A	N/A	N/A	N/A	N/A
	0-5 mm	FLSM-0-5	from powder	from powder	from powder and original sample			0-1.25 mm	
	2.5-5 mm	FLSM-2.5-5						1.25-5 mm	
	original sample	FLSM							
Kuusakoski mixed waste	0-25µm		N/A	N/A	N/A	N/A	N/A	N/A	N/A
	0-5 mm	FLKM-0-5	from powder	from powder	from powder and original sample			0-1.25 mm	
	2.5-5 mm	FLKM-2.5-5						1.25-5 mm	
	original sample	FLKM							
Estonian mixed waste	0-25µm								
	0-5 mm	EPM-0-5	from powder	from powder	from powder and original sample			0-1.25 mm	
	2.5-5 mm	EPM-2.5-5						1.25-5 mm	
	original sample	EPM							
Estonian Concrete brick	0-25µm		N/A	N/A	N/A	N/A	N/A	N/A	N/A
	0-5 mm	EACB-0-5	from powder	from powder	from powder and original sample			0-1.25 mm	
	2.5-5 mm	EACB-2.5-5						1.25-5 mm	
	original sample	EACB							
Salpamaa concrete	0-25µm								
	0-5 mm	FLSC-0-5	from powder	from powder	from powder and original sample			0-1.25 mm	
	2.5-5 mm	FLSC-2.5-5						1.25-5 mm	
	original sample	FLSC							
Latvia Concrete	0-25µm								
	0-5 mm	LSZC-0-5	from powder	from powder	from powder and original sample			0-1.25mm	
	2.5-5 mm	LSZC-2.5-5						1.25-5 mm	
	original sample	LSZC							

- **Particle size distribution measurement** and fractionation were performed using a **test sieve shaker** manufactured by Haver & Boecker. The shaker consisted of 13 sieves with aperture sizes ranging from 25 to 5000 µm, along with a pan positioned beneath the bottom sieve stack. This pan collected particles smaller than 25 µm for subsequent analysis using laser diffraction methods, as described later. The shaker operated with vibrations set to occur for 30-60 minutes, with intervals of 2 minutes, and an amplitude of 1.5. Samples weighing between 500 and 1000 grams were placed on the uppermost sieve (5mm).
- **Particle size distribution measurement** by Malvern Mastersizer 3000 using **laser diffraction particle size analyzer,** modern laser diffraction particle size analyzer utilized was the Malvern Mastersizer 3000, featuring the Hydro EV particle dispersing unit and water as the dispersant liquid (Malvern Instruments, UK).
- The alternative method employed for **particle size determination** utilized a blend of **microscopy and automated image analysis.** The instrument utilized for this analysis was the Malvern Morphologi G3 from Malvern Instruments, UK. Within this instrument, measurements were conducted through automated image analysis of microscope images of the sample. Due to the variation in particle sizes within the 0-5 mm range, it was impractical to analyze them all in a single assessment. The smallest particles required up to 5x magnification, while the largest ones couldn't fit into images at 2.5x magnification. As a result, we opted to divide the particle size range into five subcategories: 0-500 µm, 500-800 µm, 800-1250 µm, 1250-2500 µm, and 2500-5000 µm. However, all size ranges underwent analysis using additional features of a morphology analyzer. This included enabling Z stacking with an additional layer of imaging to capture larger particles from a further distance, thereby preventing the oversight of smaller particles nearby. Additionally, the analyzer stitched together pieces of large particles that couldn't fit within the specific magnification limits of imaging, especially in the case of the latter two size ranges. These ranges were beyond the equipment's applicability scope, as it effectively measures particles up to 1000 µm. This approach was consistently applied across all analyses conducted with the morphology instrument.
- **Particle morphology analysis**, The Malvern Morphologi G3 was employed to assess different attributes depicting **particle shape**. The analysis included evaluating the

morphology of particles based on mean circularity and elongation. The report also incorporates representative images depicting particle shapes. Furthermore, the morphology is visualized through scanning electron microscope (SEM) images.

- The **specific surface area** of solids was determined using a fully automated Micromeritics 3Flex surface characterization analyzer (Micromeritics Instrument Corp., USA), which employed the **Bennett-Emmett-Teller (BET) method**. This method accounts for both the inner and outer surface area of particles.
- The material's **elemental composition** was assessed using **energy-dispersive X-ray spectroscopy (EDS),** which included SEM-EDS mapping to illustrate element distribution. The SEM-EDS apparatus employed for these measurements was the Hitachi SU3500.
- The sample's **mineral composition** underwent examination through powder **X-ray diffraction (XRD)**. The objective of the XRD analysis was to identify the primary crystalline mineral phases present in the sample. This investigation utilized a Bruker D8 Advance X-ray diffractometer (Bruker Corp., Germany).
- **Thermogravimetric analysis (TGA)** was conducted to examine how the sample behaves under high temperatures. This analytical technique relies on measuring the weight loss of a material as it undergoes programmed heating. In this study, the temperature was gradually increased from room temperature to 700 °C. The thermographic analysis was performed using a Netzsch STA 449 C Jupiter thermo-microbalance (Netzsch-Gerätebau GmbH, Germany).

3. Results and discussions

This section provides an overview of the particle properties and composition of the samples, focusing on aspects such as size, shape, elemental composition, mineralogy, and thermal behavior.

3.1. Particle size distribution (PSD)

The particle size distributions of the samples were determined through sieving analysis, which served as the primary method for most materials. Laser diffraction and image analysis were employed as additional methods for a limited number of materials.

- Sieving analysis

We used sieving test method for determination of particle size distribution since most of the samples in the study were coarse. The results of particle size distribution is shown in figure. 8 for all the chosen samples. Sample EPM exhibits a notably uniform particle size distribution, whereas the remaining samples display steep slope curves, indicative of elevated levels of coarse material content present within them.

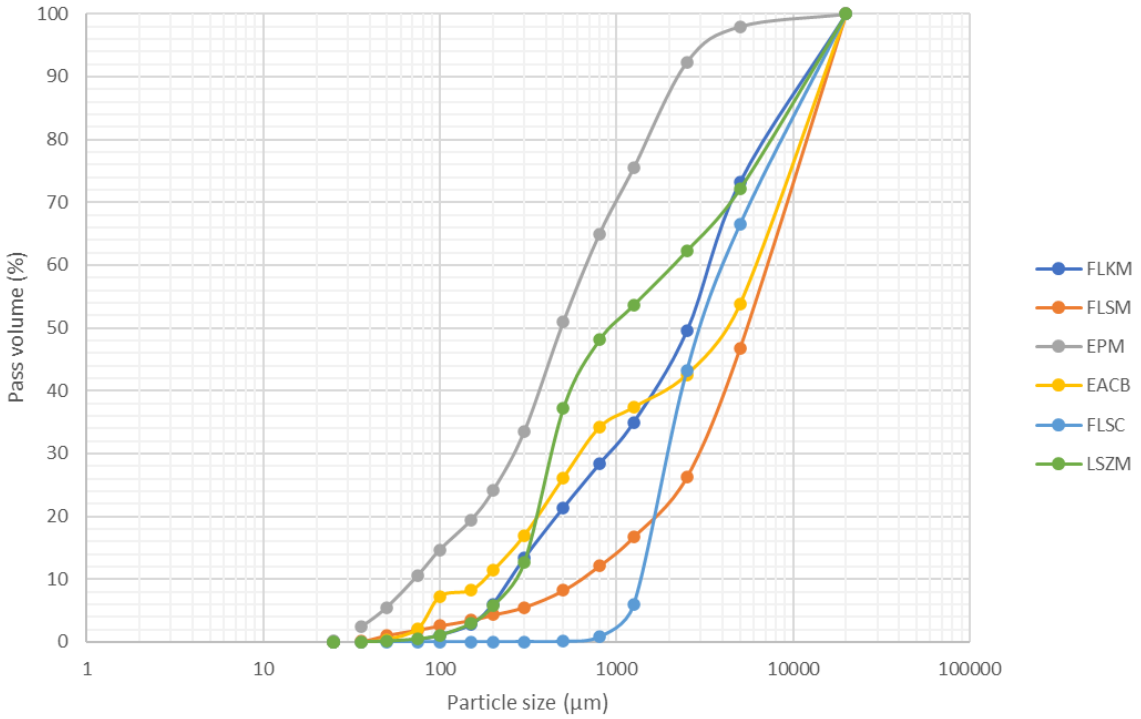

Figure 8. Cumulative particle size distribution of chosen project samples

- Laser diffraction analyzer (Malvern Mastersizer 3000)

Regarding the samples which contained particles smaller than 25 µm, we have analyzed the particle size distribution using the laser diffraction method. In this study, only one of the

samples from Estonia (mixed waste- EPM) yielded with such fine particles and the PSD is plotted as per the Figure.9.

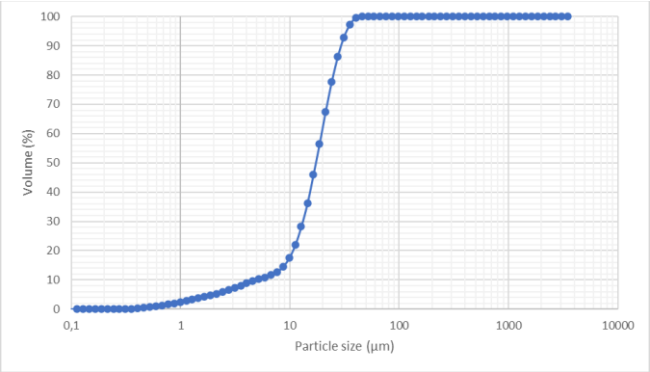

Figure 9. Cumulative particle size distribution of sample EPM

- Automated analysis of images for the measurement of PSD

Table 3 displays particle dimensions obtained from a dry sample using Malvern Morphologi G3. It's important to note that these measurements aren't directly comparable to those acquired through sieving test due to significant differences in the methodologies. The automated image analysis technique focuses on identifying individual particles within dry particles, while test sieve shaker measures volume distribution of particles passed though sieves with different aperture sizes. Our aim is to examine the dimensions of the predominant larger particles in this sample. Hence, D[4,3] emerges as the most fitting parameter for this task, as it accurately represents the size of these particles that comprise the bulk of the sample volume. This parameter is particularly sensitive to the presence of large particles within the size distribution.

Table 3. The particle sizes D10, D[3,4] (Volume moment mean diameter), D50 (median diameter), and D90 were derived from the volumetric undersize distribution of the samples analyzed using automated image analysis with the Malvern Morphologi G3.

Sample code	Size range (µm)	D10 (µm)	D[4,3] (µm)	D50 (µm)	D90 (µm)
EACB	0-500	64.99	324.9	294.8	577
	500-800	639.9	812.3	825.6	975.4
	800-1250	1143	1366	1367	1660
	1250-2500	1530	4062	1779	1909
	2500-5000	26.59	5555	56.78	99.5
EPM	0-500	66.48	348.6	324.2	650.9
	500-800	732.5	1106	934.1	1901
	800-1250	1074	1486	1425	1607
	1250-2500	1727	5732	1868	1961
	2500-5000	169.9	5065	528.6	663.1
FLKM	0-500	113.4	433.1	400.8	741.9
	500-800	648.2	951.5	1010	1333
	800-1250	1084	2003	1480	1759
	1250-2500	1120	5800	1695	1876
	2500-5000	806.3	4761	1665	1669
FLSC	0-500	139.5	420.5	440.3	691.1
	500-800	441.2	694.3	711.4	865.4
	800-1250	410.1	937.4	980.4	1289
	1250-2500	1078	5110	1776	1899
	2500-5000	566.3	8318	1553	1558
FLSM	0-500	48.19	304.4	241.4	680
	500-800	752.3	1229	1200	1870
	800-1250	1057	1998	1437	1858
	1250-2500	1024	2960	1705	1741
	2500-5000	724.4	5464	1541	1695
LSZM	0-500	47.42	252.4	239.6	479.2
	500-800	714.6	1287	953	1180
	800-1250	1152	1383	1193	1754
	1250-2500	1513	4187	1800	1889
	2500-5000	1544	5247	1547	1550

3.2. Morphology analysis

Particle shape analysis was conducted using a combination of microscopy and image analysis with the Malvern Morphologi G3.

3.2.1. Automated image analysis

Table. 4 depicts the morphology of particles by employing the average circularity and elongation values. Circularity refers to how close an object's shape is to a perfect circle, with a value of 1 indicating a perfect circle. Elongation, on the other hand, measures how stretched or

elongated an object is compared to a perfect circle, with higher values indicating greater elongation.

Table 4. The average circularity and elongation of particles within the examined samples

Sample code	Size range (µm)	Circularity (-)	Elongation (-)
EACB	0-500	0.5416	0.2927
	500-800	0.9028	0.2138
	800-1250	0.8809	0.2313
	1250-2500	0.5743	0.3661
	2500-5000	0.7712	0.1543
EPM	0-500	0.3435	0.376
	500-800	0.7946	0.2927
	800-1250	0.7732	0.2237
	1250-2500	0.3299	0.4372
	2500-5000	0.5649	0.4111
FLKM	0-500	0.5464	0.366
	500-800	0.6171	0.3088
	800-1250	0.5687	0.4064
	1250-2500	0.3786	0.4773
	2500-5000	0.6564	0.3725
FLSC	0-500	0.6955	0.2476
	500-800	0.8817	0.205
	800-1250	0.8542	0.2469
	1250-2500	0.5851	0.402
	2500-5000	0.6906	0.403
FLSM	0-500	0.4045	0.371
	500-800	0.6494	0.4082
	800-1250	0.5795	0.5136
	1250-2500	0.6394	0.2674
	2500-5000	0.5933	0.3226
LSZM	0-500	0.7496	0.2441
	500-800	0.8644	0.3642
	800-1250	0.8728	0.2009
	1250-2500	0.5521	0.3886
	2500-5000	0.7574	0.3607

The distributions of circularity and elongation based on both number and volume of the samples are provided in Appendix 2. The x-axes of the graphs represent circularity and elongation, with a consistent range from 0 to 1. While the y-axis ranges vary based on peak heights, the overall shape of the distribution is emphasized over exact peak percentages. Moreover, certain volume-based distributions exhibit a few distinct peaks, likely due to the

presence of large particles or particle aggregates, exemplified by all samples with aperture size ranges between 2500-5000 µm. In such instances, the number distribution offers a more realistic depiction of particle shapes within the sample. Additionally, particle morphology can be assessed through microscope images of particles, as demonstrated in Appendix 1. On an average basis, particles within Concrete brick samples tend to be more circulated than elongated, fraction of 1250-2500 µm of all tend to be slightly more elongated than other fractions in all samples except FLSM which is more circulated.

3.2.2. Scanning electron microscopy analysis (SEM)

Particle morphology of large samples cannot be visually assessed using scanning electron microscopy (SEM) without prior treatment. Therefore, we prepared a fine powder from the 0-5 mm and 2.5-5 mm fractions of each sample. We used a hammer mill for harder materials like concrete brick and ball mills for mixed wastes containing softer materials like wood, plastic, and wool. This powder was then analyzed using SEM, followed by EDS for elemental composition analysis. Table 5 summarizes the results of the SEM study, with varying magnifications used for each sample to enhance visual clarity.

Table 5. SEM imaging analysis of samples

Sample code	Fraction	SEM images	
FLSM-0-5	0-5 mm	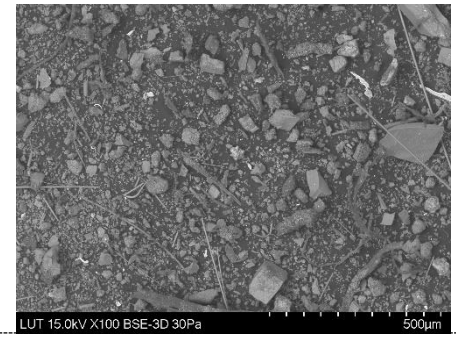	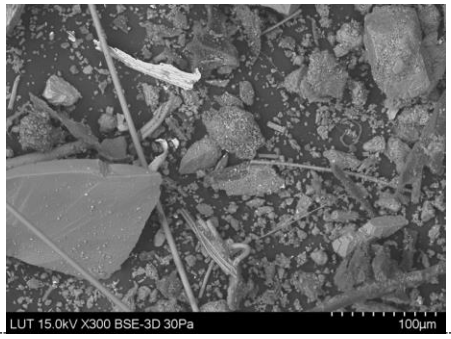

FLSM-2.5-5	2.5-5 mm	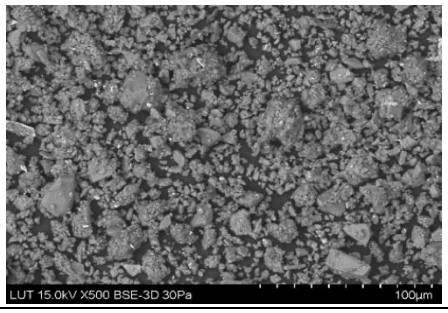	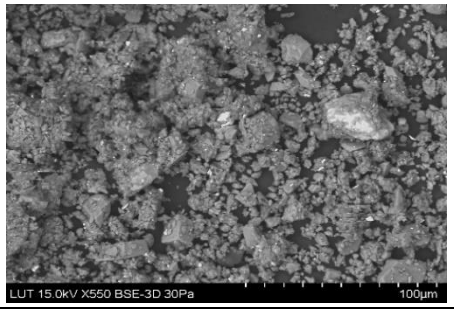
FLKM-0-5	0-5 mm	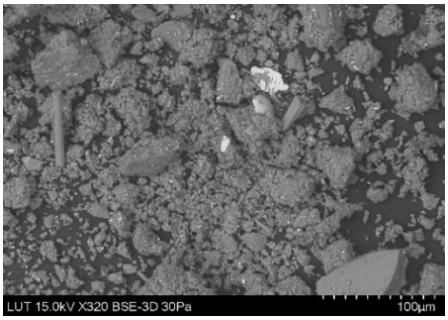	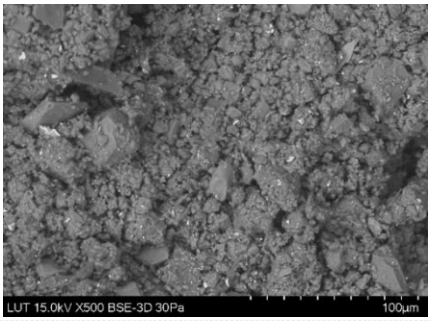
FLKM-2.5-5	2.5-5 mm	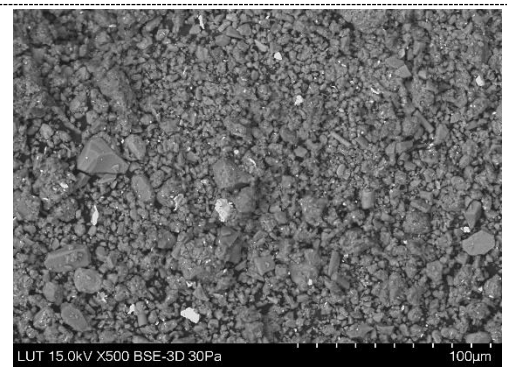	
FLSC-0-5	0-5 mm	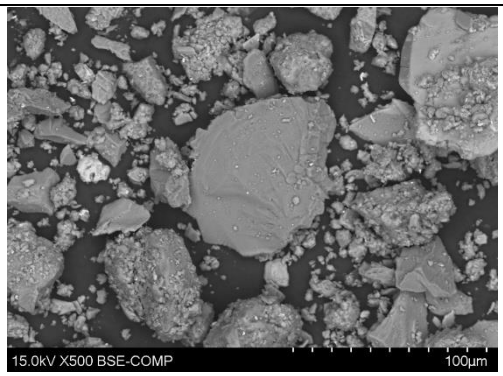	

FLSC-2.5-5	2.5-5 mm	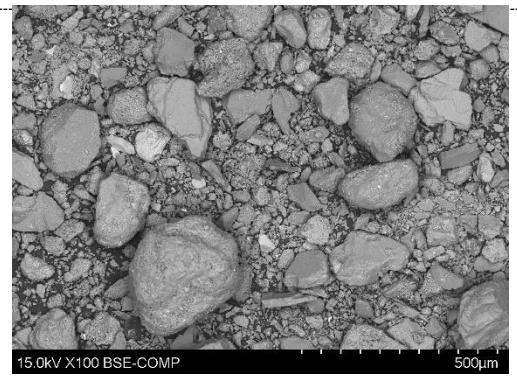
LSZM-0-5	0-5 mm	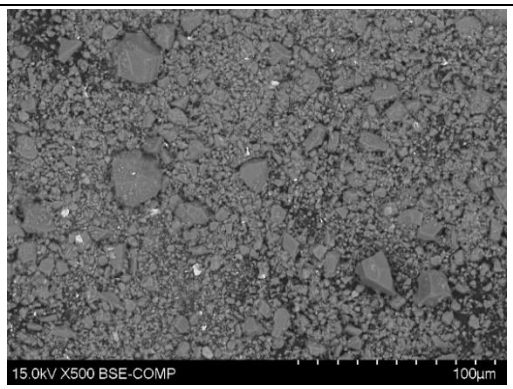
LSZM-2.5-5	2.5-5 mm	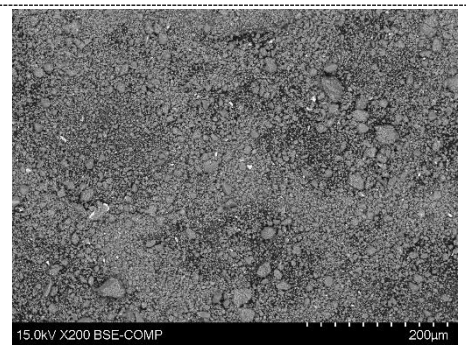 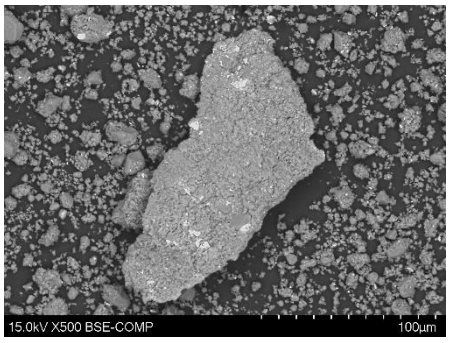
EPM-0-5	0-5 mm	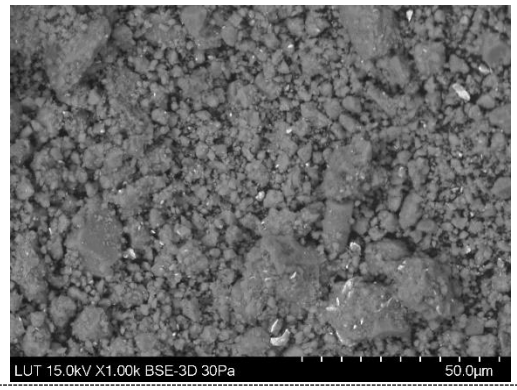

EPM-2.5-5	2.5-5 mm	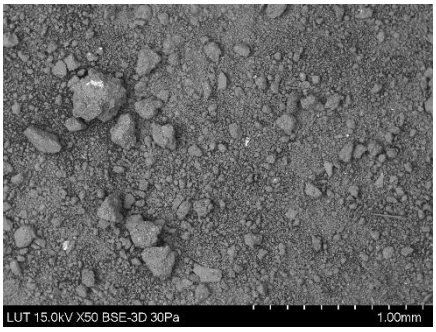	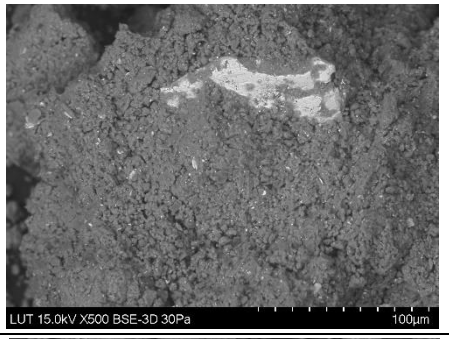
EACB-0-5	0-5 mm	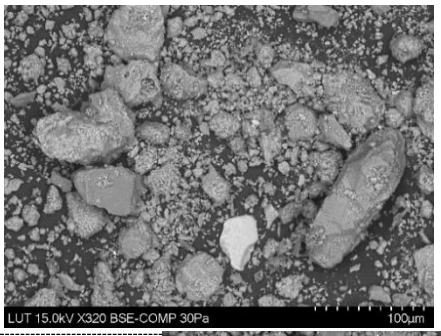	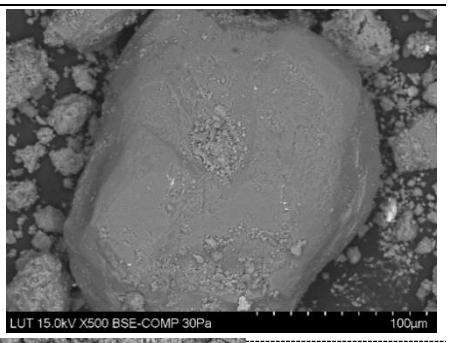
EACB-2.5-5	2.5-5 mm	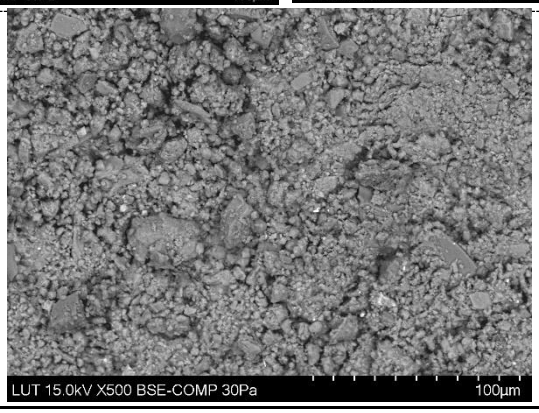	

As previously mentioned, SEM images do not offer much information about particle morphology because the original shape of the particles has been altered or damaged during the milling process.

Nevertheless, it is apparent that the treated product retains a heterogeneous nature, with distinct materials discernible within each sample. Generally, the fraction 2.5-5 mm of mixed wastes exhibits a more uniform appearance due to a higher prevalence of wood and soft materials, as opposed to the 0-5 mm fraction, which contains a mix of both soft and hard materials. In the case of harder samples like FLSC and EACB, the composition appears more homogeneous, typically consisting of one or two types of materials. Sample FLSM-0-5 displayed remarkable resistance to milling, as evidenced by the intact and unbroken fibers observed within the sample.

3.3. Specific surface area measurement using Bennett-Emmett-Teller (BET) method

Surface area can be estimated using particle size distributions by assuming regular geometric shapes for the particles, such as the "equivalent spherical diameter." However, this method does not account for the surface texture of the particles (Mucsi et al., 2021, p. 3416). The measurement of BET specific surface area (SSA) is a well-recognized and commonly employed technique for assessing the SSA of solid materials, particularly those with open porosity. According to the results summarized in table 6. As evident from the table, samples of concrete bricks from Salpamaa and Estonia in the 0-5 mm fraction exhibit the highest specific surface areas, as determined by the BET method, with values of 33.7 and 15.8 m^2/g, respectively. Within the mixed waste category, the 0-5 mm fraction from Estonia demonstrates the highest specific surface area (SSA), with a value of 10.7 m^2/g.

Table 6. Specific surface area measured using BET method

Sample	Fraction	Sample code	BET SSA (m2/g)
Salpamaa mixed waste	0-5 mm	FLSM-0-5	2.5
	2.5-5 mm	FLSM-2.5-5	4.3
Kuusakoski mixed waste	0-5 mm	FLKM-0-5	6.4
	2.5-5 mm	FLKM-2.5-5	7.1
Salpamaa concrete brick	0-5 mm	FLSC-0-5	33.7
	2.5-5 mm	FLSC-2.5-5	12.2
Latvia mixed waste	0-5 mm	LSZM-0-5	2.7
	2.5-5 mm	LSZM-2.5-5	1.2
Estonian mixed waste	0-5 mm	EPM-0-5	10.7
	2.5-5 mm	EPM-2.5-5	7.4
Estonian Concrete brick	0-5 mm	EACB-0-5	15.8
	2.5-5 mm	EACB-2.5-5	15.1

3.4. Elemental composition analysis using energy-dispersive X-ray spectroscopy (EDS) method

As mentioned earlier in the SEM section, given the heterogeneous nature of all samples, each contained a variety of materials. To streamline analysis, we selected one point representative from each material within the sample based on visual similarities in color or shape. Table 7 listed the elemental (chemical compositions) which were detected in different factions within samples where elements O, Si, Ca, Al, and Fe is detected in almost all samples.

Table 7. Elemental composition of samples analyzed by EDS method

		Element (Wt%)																	
Sample code	**Fraction**	**C**	**O**	**F**	**Na**	**Mg**	**Al**	**Si**	**P**	**S**	**Cl**	**K**	**Ca**	**Ti**	**Cr**	**Mn**	**Fe**	**Cu**	**Co**
FLSM-0-5	0-5 mm (1)	41.8	31.4	2	0.9	0.6	2.3	9.6	-	-	0.9	0.5	6.7	-	-	-	-	-	-
FLSM-0-5	0-5 mm (2)	22.6	8.1	-	0.7	0.5	1.2	4.2	-	-	0.5	0.3	3.9	-	6.7	0.1	48.3	-	0.7
FLSM-0-5	0-5 mm (3)	53	12.8	0.5	3.5	0.7	1.1	3.1	0.6	-	5.1	-	8.2	-	0.1	-	-	-	0.3
FLSM-0-5	0-5 mm (4)	-	45.3	-	1.6	1.1	2.4	7.7	-	-	-	0.6	27.5	-	-	-	2.3	-	-
FLSM-2.5-5	2.5-5 mm (1)	-	34	-	5	1.4	4.3	26.5	-	-	0.8	-	11.8	-	0.5	-	6	-	0
FLSM-2.5-5	2.5-5 mm (2)	-	29.8		1.7	0.5	1.7	5.6	-	-	4.6	-	2.6	-	-	-	51.3	-	-
FLSM-2.5-5	2.5-5 mm (3)	-	32.2	-	4.6	1.2	4.8	23.6	-	-	0.9	-	12.6	-	0.7	-	7.7	-	0.1
FLKM-0-5	0-5 mm (1)	-	31	-	1.8	1	4.1	21.5	-	5.9	-	-	17.7	-	0.9	0.1	8.7	-	0.06
FLKM-0-5	0-5 mm (2)	-	28.3	-	1.8	1.15	4.8	20.4	-	5.7	-	-	17.3	-	1.3	0.1	12	-	0.2
FLKM-2.5-5	2.5-5 mm (1)	-	35.7	-	2.7	0.8	4.7	21.9	-	4.8	-	-	13.3	-	0.9	-	7.3	-	0
FLKM-2.5-5	2.5-5 mm (2)	-	2.7	-	0.8	0.2	1.8	6.2	-	-	-	3.2	-	-	11.5	0	70	-	-
FLKM-2.5-5	2.5-5 mm (3)	-	27.7	-	2.4	0.8	6.5	23.7	-	5.4	-	-	14.1	-	0.1	0.1	8.3	-	0
FLSC-0-5	0-5 mm (1)	28.2	34.8	-	0.9	0.65	4	16.2	-	0.2	-	1.8	9.5	0.2	-	-	3.6	-	-

Sample code	Fraction	Element (Wt%)																	
		C	O	F	Na	Mg	Al	Si	P	S	Cl	K	Ca	Ti	Cr	Mn	Fe	Cu	Co
FLSC-0-5	0-5 mm (2)	18.7	37.1	-	1.2	0.8	4.6	17.6	-	0.3	-	2.1	13.9	0.2	-	-	3.1	0.4	
FLSC-0-5	0-5 mm (3)	10	42.9	-	0.3	0.2	1.5	39.9	-	-	-	0.6	3.5	-	-	-	1.1	-	-
FLSC-2.5-5	2.5-5 mm (1)	11.5	38	-	1.4	0.6	6.1	23.3	-	0.4	-	3.3	11.5	0.4	-	-	3.4	-	-
FLSC-2.5-5	2.5-5 mm (2)	15.3	37.3	-	1.4	0.8	5.8	20.5	-	0.3	-	2.3	11.8	0.3	-	-	4.2	-	-
LSZM-0-5	0-5 mm (1)	-	43.3	-	0.8	0.5	2.7	37.2	-	-	-	1.3	11.8	-	-	-	2.3	-	-
LSZM-0-5	0-5 mm (2)	20.7	39.1	-	0.5	0.3	2	26.5	-	-	-	1	7.9	0.1	-	-	1.8	-	-
LSZM-0-5	0-5 mm (3)	-	2.2		0.3	0.2	1.2	11.4	-	-	-	0.4	3.8	-	9.9	0.6	69.9	-	-
LSZM-0-5	0-5 mm (4)	-	39.7	-	0.7	1.4	2	45.8	-	-	-	0.6	6	0.4	-	-	3.6	-	-
LSZM-2.5-5	2.5-5 mm (1)	27.3	33.6	-	0.7	0.4	2.2	23.2	-	-	-	1	7.1	0.1	0.4	-	3.5	0.5	-
LSZM-2.5-5	2.5-5 mm (2)	14.3	32	-	0.9	0.5	2.8	32.3	-	-	-	1.4	10.2	0.1	0.5	-	4.6	-	-
EPM-0-5	0-5 mm (1)	-	21.2	-	0.8	0.6	1.6	9	-	-	-	0.4	5.8	-	0.2	-	58.8	-	-
EPM-0-5	0-5 mm (2)	-	33	-	0.5	0.8	3.5	29.8	-	-	-	2	19.7	-	0.5	0.1	5.3	-	0
EPM-0-5	0-5 mm (3)	-	33.8	-	0.9	0.8	3.2	24.1	-	-	-	-	18.1	-	1	-	8	-	0
EPM-0-5	0-5 mm (4)	-	37.2	-	1	1.1	3.6	26	-	-	-	1.6	18.4	-	0.5	-	5.2	-	0.1
EPM-2.5-5	2.5-5 mm (1)	5.9	3.7	-	0.3	0.3	1.5	4.3	-	-	-	0.2	4.4	-	10.3	0.1	64.8	-	0.5
EPM-2.5-5	2.5-5 mm (2)	-	36	-	1.7	1.2	3.4	19	-	-	-	-	21.3	-	1.2	-	7.8	-	0.2
EPM-2.5-5	2.5-5 mm (3)	7.4	4.2	-	-	0.2	0.9	3.9	-	-	-	0.2	3.6	-	9.9	0	68.1	-	0.4
EACB-0-5	0-5 mm (1)	-	45.9	2.2	0.3	0.6	2.4	6.7	-	-	-	-	35.5	-	-	-	-	-	-
EACB-0-5	0-5 mm (2)	14.4	41.6	1.1	-	-	0.9	35.3	-	-	-	-	5	-	-	-	-	-	-
EACB-0-5	0-5 mm (3)	-	32.2	1.7	0.8	1.8	7.8	16.4	-	-	0.5	-	-	-	-	-	-	-	2.6
EACB-0-5	0-5 mm (4)	14.4	41.5	1.1	0.1	0.3	1.3	31.2	-	-	-	-	7.3	-	-	-	-	-	-
EACB-0-5	0-5 mm (5)	-	37.6	3.8	-	0.3	1.2	4	14.3	-	-	0.6	36.4	-	-	-	1.4	-	0
EACB-2.5-5	2.5-5 mm (1)	-	37.4	0	0.6	0.9	2.5	10.7	-	0.4	-	-	36.5	-	-	-	-	-	-
EACB-2.5-5	2.5-5 mm (2)	-	19.5	0	-	3.4	5.2	13.9	-	-	-	-	30	-	-	-	-	-	1.4
EACB-2.5-5	2.5-5 mm (3)	-	40	1.8	-	0.4	1.8	5.3	-	-	-	-	44	-	-	-	-	-	-
EACB-2.5-5	2.5-5 mm (4)	-	32.5	0	-	0.6	3	11.4	-	-	-	-	38.5	-	-	-	-	-	0.2

3.5. Mineral composition analysis using X-ray diffraction (XRD) method

We utilized XRD to investigate the mineral composition of the materials. To facilitate this analysis, we plotted XRD figures of the hard samples (concrete brick) and the mixed waste samples which include both soft and hard materials separately for comparison. The diffractograms depicted in Figures 10-11 illustrate the primary crystalline phases identified within the materials.

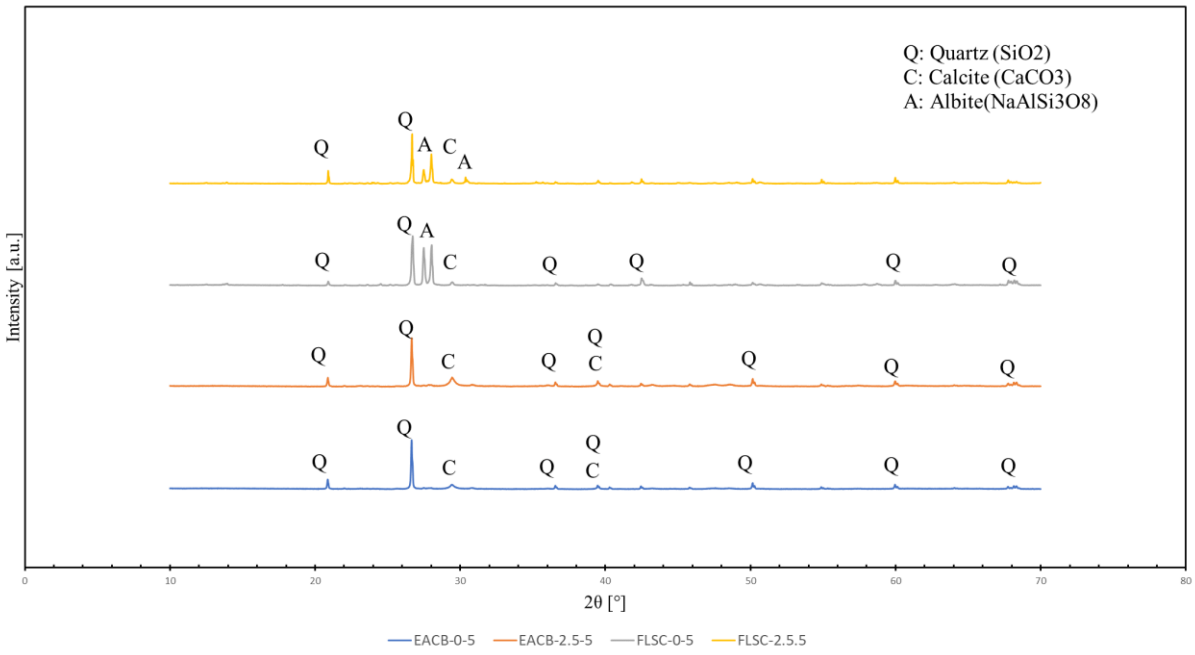

Figure 10. XRD diffractograms of hard samples (concrete brick, glass samples)

Every sample regardless of its composition being hard or mixed, were noted to contain crystalline structures such as quartz (SiO2) and calcite (CaCO3). The distinctive- presence of Albite (NaAlSi3O8) was seen only in samples from Finland. However, portlandite (Ca(OH)2) was discerned just in the Kuusakoski samples. When we look at the XRD spectra of all the other samples, not finding any reflections of portlandite (Ca(OH)2) hints that the cement element in those samples may be aging considerably. Since portlandite likely having undergone carbonation (as evidenced by the presence of CaCO3 in the XRD results) (Villaquirán-Caicedo and Mejía De Gutiérrez, 2021, vol. 281).

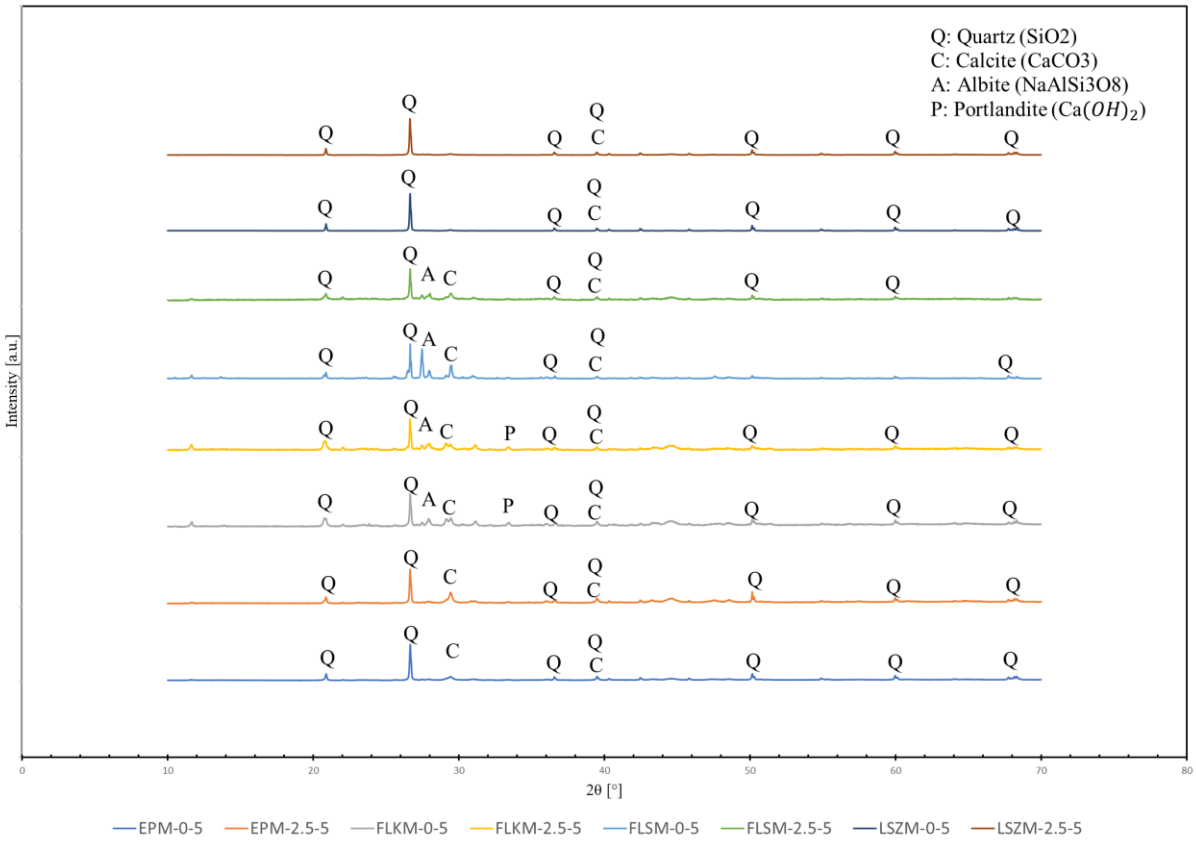

Figure 11. XRD diffractograms of mixed waste samples (mixed concrete brick with soft materials such as plastic, wood,…)

The summary of minerals based on the crystalline phases detected within each sample are listed in table 8.

Table 8. The mineral compositions of the samples determined by XRD analysis

Sample	Fraction	Sample code	Minerals
Salpamaa mixed waste	0-5 mm	FLSM-0-5	Quartz (SiO_2), Calcite ($Ca(CO)_3$). Albite ($NaAlSi_3O_8$)
	2.5-5 mm	FLSM-2.5-5	Quartz (SiO_2), Calcite ($Ca(CO)_3$). Albite ($NaAlSi_3O_8$)
Kuusakoski mixed waste	0-5 mm	FLKM-0-5	Quartz (SiO_2), Calcite ($Ca(CO)_3$). Albite ($NaAlSi_3O_8$), Portlandite ($Ca(OH)_2$)
	2.5-5 mm	FLKM-2.5-5	Quartz (SiO_2), Calcite ($Ca(CO)_3$). Albite ($NaAlSi_3O_8$), Portlandite ($Ca(OH)_2$)
Salpamaa concrete brick	0-5 mm	FLSC-0-5	Quartz (SiO2), Calcite (Ca (CO)3). Albite (NaAlSi3O8)
	2.5-5 mm	FLSC-2.5-5	Quartz (SiO_2), Calcite ($Ca(CO)_3$). Albite ($NaAlSi_3O_8$)
Latvia mixed waste	0-5 mm	LSZM-0-5	Quartz (SiO_2), Calcite ($Ca(CO)_3$)
	2.5-5 mm	LSZM-2.5-5	Quartz (SiO_2), Calcite ($Ca(CO)_3$)
Estonian mixed waste	0-5 mm	EPM-0-5	Quartz (SiO_2), Calcite ($Ca(CO)_3$)
	2.5-5 mm	EPM-2.5-5	Quartz (SiO_2), Calcite ($Ca(CO)_3$)
Estonian Concrete brick	0-5 mm	EACB-0-5	Quartz (SiO_2), Calcite ($Ca(CO)_3$)
	2.5-5 mm	EACB-2.5-5	Quartz (SiO_2), Calcite ($Ca(CO)_3$)

3.6. Thermogravimetric analysis (TGA)

Figures 12-15 illustrate the findings of the thermogravimetric analysis. To further compare soft and hard waste materials, we plotted the TG and DTG curves separately for the hard samples (concrete bricks) and mixed waste samples. As the mass changes, a DTG curve shows the rate of decomposition of the sample's components, whereas TG curves show the amount of mass changes as a function of temperature (Wang et al., 2024, vol. 733).

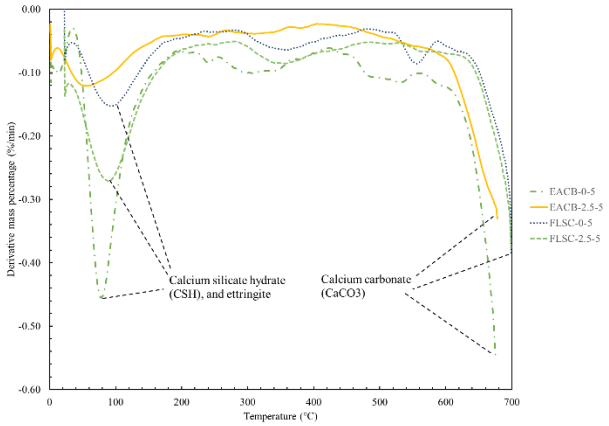

Figure 13. DTG curves of concrete brick CDW

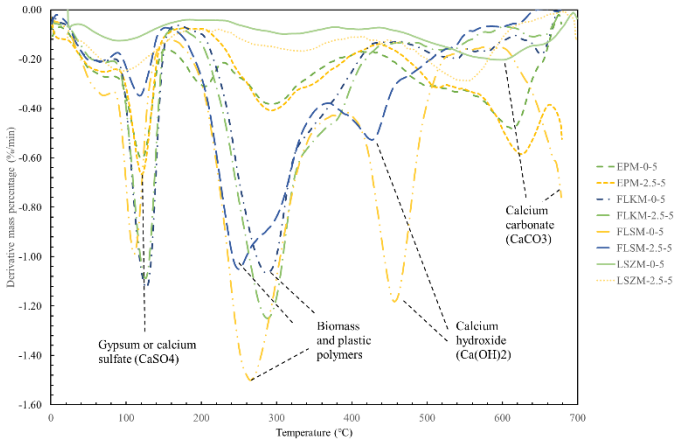

Figure 12. DTG curves of mixed CDW

Concrete brick samples show a first peak in DTG at about 100 ºC due to the decomposition of ettringite and C-S-H. Mixed samples have a peak of gypsum (CaSO4·2H2O) around 150 ºC. Their peaks are partially overlapped in TGA, which makes it difficult to clearly identify them (Wang et al., 2024, vol. 733). Mixed waste thermograms, especially those from Finland, tend to have two or three peaks/shoulders, excluding moisture evaporation peaks. Cellulosic degradation occurs at 200-400°C, while plastic degradation occurs at 400-600°C. Due to overlapping reactions at similar decomposition temperatures, the TG–DTG curves of individual components in a mixture cannot be distinguished, especially in heterogeneous mixtures. However, due to large amount of biomass and plastic in Finnish mixed wastes (salpamaa and kuusakoski), it is expected that one peak is showing the presence of biomass mixtures including cellulose, hemicellulose, and lignin. Between 200 and 400°C, major biomass materials degrade with a Tp ranging between 355 and 370°C. The other peak represents the breakdown of PE, PP, PET, and PVC, which are the most prevalent postconsumer plastic polymers. In general, these plastic polymers degrade in a single narrow DTG shoulder, with the exception of PVC, which degrades in two steps (Gerassimidou et al., 2020, p. 942). A peak occurs between 550 to 850 °C in concrete brick samples, caused by CaCO3 decomposition (Wang et al., 2024, vol. 733).

The mass loss of both concrete brick samples and mixed waste samples, due to the loss of non-evaporable water (between 105 °C and 550 °C) and the decomposition of CaCO3 (between 550 °C and 700 °C), are presented in TG curves.

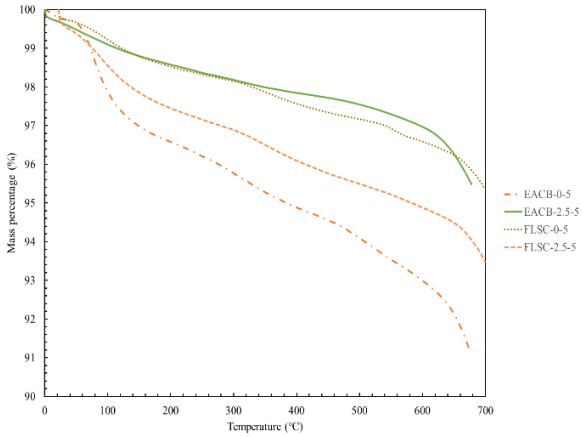

Figure 14. TG curves of concrete brick CDW

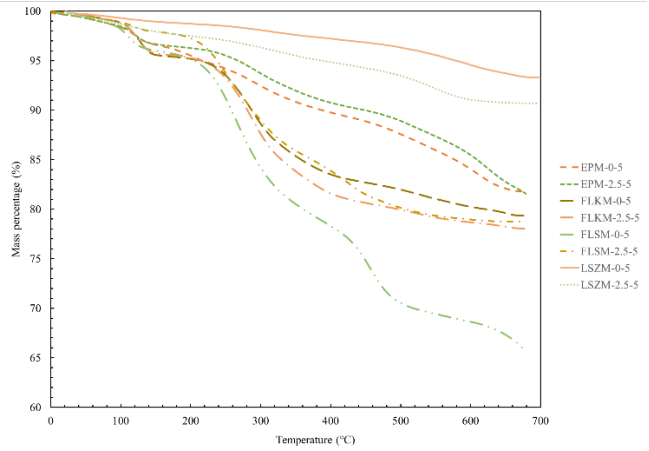

Figure 15. TG curves of mixed CDW

TGA analysis can determine some hydrated compounds of cement. In the range of 105 to 550ºC, the mass loss is due to non-evaporating water, while between 550 and 700ºC, the mass loss is caused by CaCO3 decomposition. Cwater and CCaCO3 can then be calculated as follows:

$$Cwater = M105 \circ C - M550 \circ C$$

$$CCaCO3 = (100.09/44.01) * (M550 \circ C - M700 \circ C)$$

Where M (T ºC) (T=105, 550, and 850 ºC) is a sample mass (%) obtained from the TG curve at temperature T ºC, and ratio 100.09/44.01 corresponds to the molar mass ratio of CaCO3/CO2. A summary of the water and CaCO3 contents of all samples is provided in table 9.

Table 9. Water content and calcium carbonate content of samples in percentage

Sample	Fraction	Sample code	C_{water} (%)	C_{CaCO3} (%)
Salpamaa mixed waste	0-5 mm	FLSM-0-5	28.9	9.2
	2.5-5 mm	FLSM-2.5-5	19.5	1.9
Kuusakoski mixed waste	0-5 mm	FLKM-0-5	17.7	4.7
	2.5-5 mm	FLKM-2.5-5	19.6	3.2
Salpamaa concrete brick	0-5 mm	FLSC-0-5	2.2	3.2
	2.5-5 mm	FLSC-2.5-5	3.6	3.9
Latvia mixed waste	0-5 mm	LSZM-0-5	3.7	5.2
	2.5-5 mm	LSZM-2.5-5	6.4	3.4
Estonian mixed waste	0-5 mm	EPM-0-5	12	11.1
	2.5-5 mm	EPM-2.5-5	10.7	14.5
Estonian Concrete brick	0-5 mm	EACB-0-5	4.5	6
	2.5-5 mm	EACB-2.5-5	1.8	4.4

4. Conclusions

This study examines construction and demolition waste (CDW), comprising mixed concrete and ceramic screenings, as well as recycled aggregates, to evaluate its suitability as a raw material for stormwater filtration production. The flow and filtration properties depend largely on the measured characteristics. Particle size distribution, specific surface area, and particle morphology measurements revealed the physical properties of CDW samples for a better understanding of filter performance in terms of flowability and filtration of stormwater through the samples. Samples which have a highly even distributed particles are supposed to better let the stormwater flow through. Moreover, there may be a correlation between median size and specific surface area, as smaller particles typically have higher surface area due to their increased surface-to-volume ratio. A higher specific surface area can enhance filtering efficiency by providing more surface area for interactions between the particles and the fluid being filtered. The higher specific surface area enhances the adsorption properties and helps the filter media to remove the pollution from the stormwater. Particle morphology can also give

ideas about the filter behaviour in flowing the stormwater. Elemental and mineral composition measured by SEM-EDS, and XRD as well as thermal behaviour analysed by TGA acknowledged the chemical composition of the CDW samples which gives information about potentially hazardous elements, pollution, and the organic/inorganic ratio. The research findings have resulted in the following conclusions.

In this study, sample EPM from Estonia has the more consistent particle size distribution, contrasting with the other samples showing steep slope curves, indicating a higher content of coarse materials. The morphology analysis reveals that particles in concrete brick samples are in general more circular rather than mixed waste samples When particles have similar shapes across different fractions, the filter is expected to perform better. This is because consistent particle shapes create efficient void spaces that leads to less pressure drop and allows fluid to flow evenly through the filter.

Despite the altered shapes, the treated samples exhibit a heterogeneous nature, with distinct materials present in each sample. The 2.5-5 mm fraction of mixed wastes appears more uniform due to the prevalence of wood and soft materials, while the 0-5 mm fraction contains a mix of soft and hard materials. Harder samples like FLSC and EACB show a more homogeneous composition. FLSM-0-5 demonstrates high resistance to milling, with intact fibres. Specific surface area analysis using the BET method reveals that concrete bricks from Salpamaa and Estonia in the 0-5 mm fraction have the highest specific surface areas. Estonian mixed waste in fraction of 0-5 mm shows the highest specific surface area among mixed CDWs. Elemental analysis detects O, Si, Ca, Al, and Fe in almost all samples.

The analysis of the investigated materials using XRD revealed that all samples predominantly consist of quartz and calcite. Additionally, small quantities of Albite were present in all Finnish samples. Portlandite was identified in both fractions from Kuusakoski, likely since it has not undergone transformation into calcite due to carbonation processes over time. Finnish samples exhibited a significant presence of biomass and plastic, as evidenced by peaks observed in TGA curves, and generally higher water content in Finnish mixed samples compared to CaCO3 content. Conversely, the values for concrete brick samples from salpamaa, and Estonia, were

found to have less water content which is an indicator for lower number of organic matters in samples.

References

Ahmad, T., Ahmad, K., Ahad, A., Alam, M., 2016. Characterization of water treatment sludge and its reuse as coagulant. Journal of environmental management 182, 606–611. https://doi.org/10.1016/j.jenvman.2016.08.010

El-taweel, R.M., Mohamed, N., Alrefaey, K.A., Husien, S., Abdel-Aziz, A.B., Salim, A.I., Mostafa, N.G., Said, L.A., Fahim, I.S., Radwan, A.G., 2023. A review of coagulation explaining its definition, mechanism, coagulant types, and optimization models; RSM, and ANN. Current Research in Green and Sustainable Chemistry 6, 100358. https://doi.org/10.1016/j.crgsc.2023.100358

Gan, Y., Li, J., Zhang, L., Wu, B., Huang, W., Li, H., Zhang, S., 2021. Potential of titanium coagulants for water and wastewater treatment: Current status and future perspectives. Chemical Engineering Journal 406, 126837. https://doi.org/10.1016/j.cej.2020.126837

Gerassimidou, S., Velis, C.A., Williams, P.T., Komilis, D., 2020. Characterisation and composition identification of waste-derived fuels obtained from municipal solid waste using thermogravimetry: A review. Waste Management & Research: The Journal for a Sustainable Circular Economy. https://doi.org/10.1177/0734242x20941085

Luukkonen, T., Tolonen, E.-T., Runtti, H., Pellinen, J., Hu, T., Rämö, J., Lassi, U., 2014. Removal of total organic carbon (TOC) residues from power plant make-up water by activated carbon. Journal of Water Process Engineering 3, 46–52. https://doi.org/10.1016/j.jwpe.2014.08.005

Mucsi, G., Halyag Papné, N., Ulsen, C., Figueiredo, P.O., Kristály, F., 2021. Mechanical Activation of Construction and Demolition Waste in Order to Improve Its Pozzolanic Reactivity. ACS Sustainable Chemistry & Engineering. https://doi.org/10.1021/acssuschemeng.0c05838

Teng, T.T., San Wong, S., Wei Low, L., 2014. Chapter 10 - Coagulation–Flocculation Method for the Treatment of Pulp and Paper Mill Wastewater, The Role of Colloidal Systems in Environmental Protection. Elsevier, Amsterdam. https://doi.org/10.1016/B978-0-444-63283-8.00010-7

Villaquirán-Caicedo, M.A., Mejía De Gutiérrez, R., 2021. Comparison of different activators for alkaline activation of construction and demolition wastes. Construction and Building Materials. https://doi.org/10.1016/j.conbuildmat.2021.122599

Wang, C., Chazallon, C., Braymand, S., Hornych, P., 2024. Thermogravimetric analysis (TGA) for characterization of self-cementation of recycled concrete aggregates in pavement. Thermochimica Acta. https://doi.org/10.1016/j.tca.2024.179680

Zhang, M., Yao, J., Wang, X., Hong, Y., Chen, Y., 2019. The microbial community in filamentous bulking sludge with the ultra-low sludge loading and long sludge retention time in oxidation ditch. Scientific Reports. https://doi.org/10.1038/s41598-019-50086-3

Appendices

Appendix 1:

Table 10. Morphology images of studied samples

Sample code	Size range (µm)	Morphology images
EACB	0-500	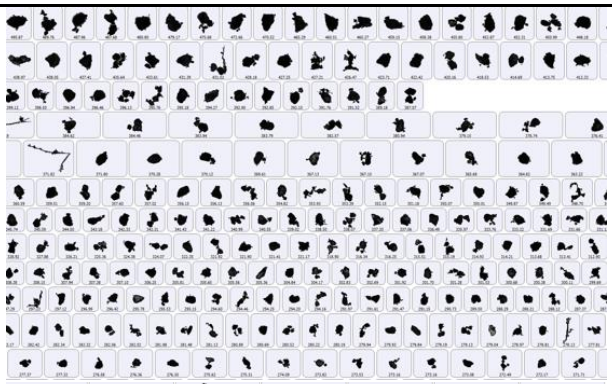
	500-800	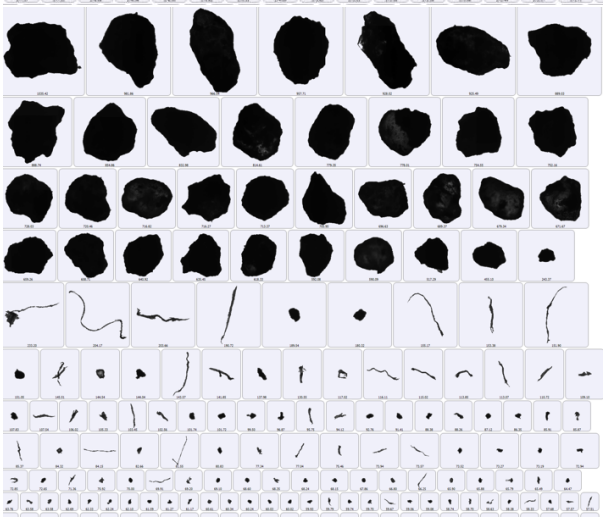
	800-1250	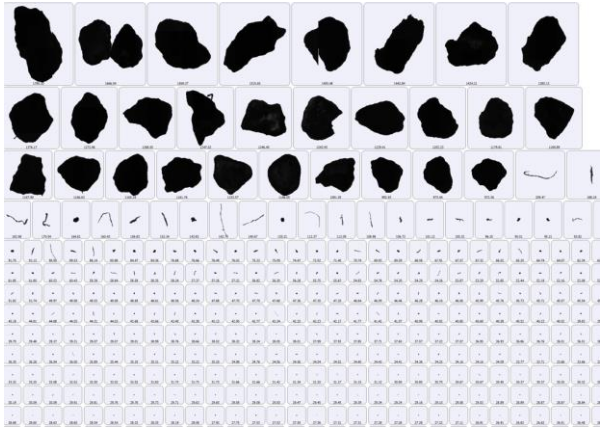

1250-2500

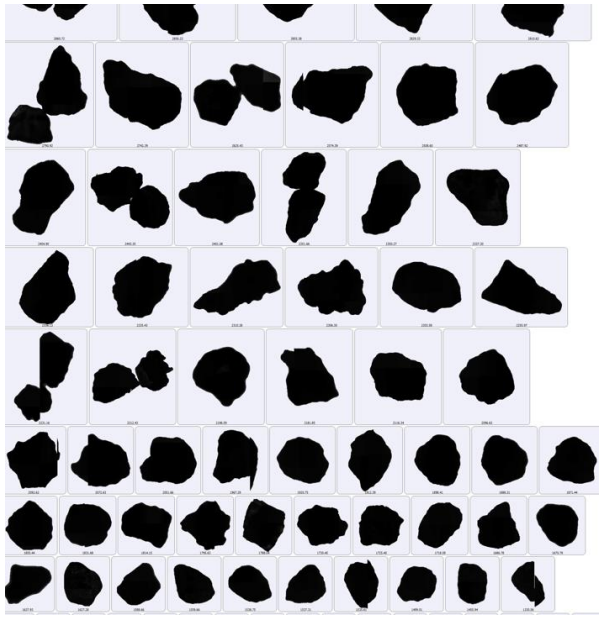

2500-5000

	0-500	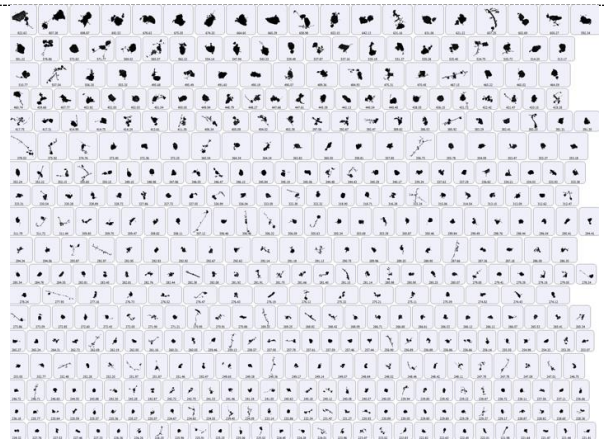
EPM	500-800	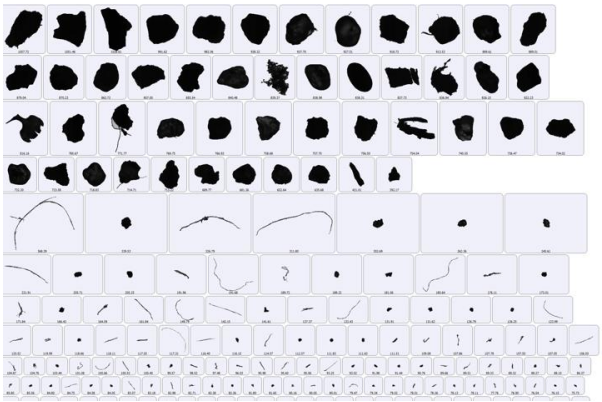
	800-1250	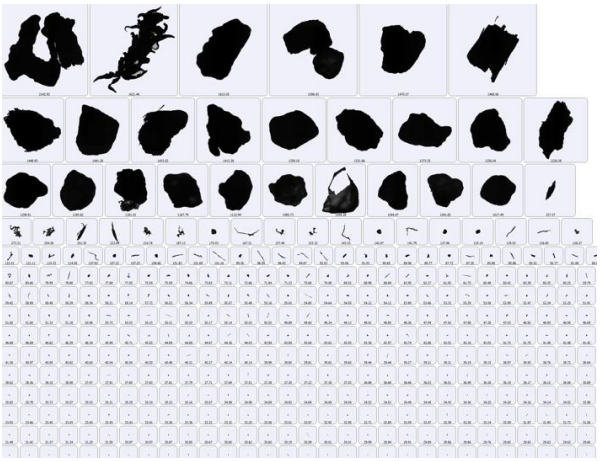

1250-2500

2500-5000

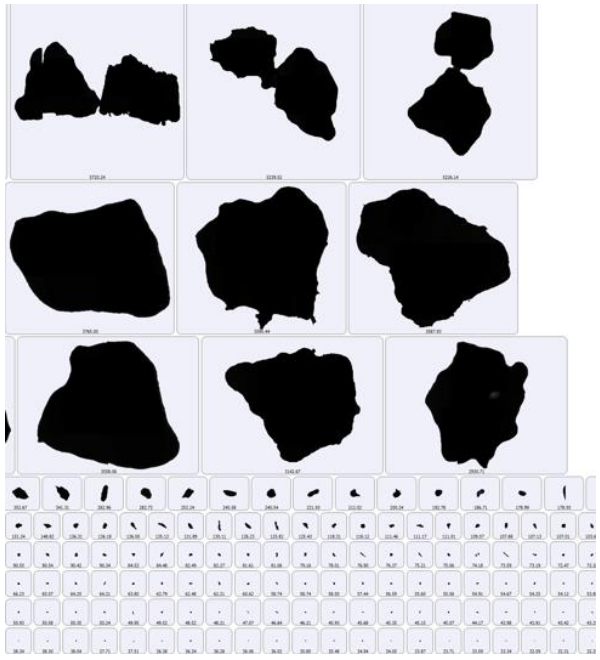

FLKM

0-500

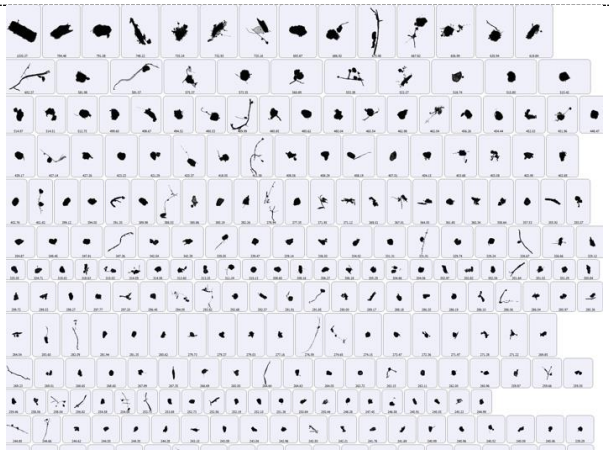

500-800

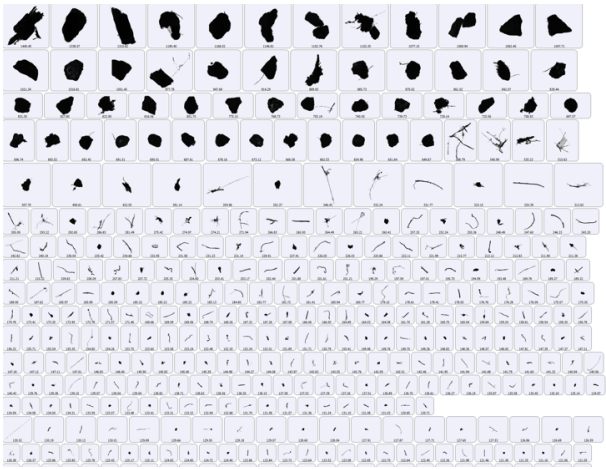

800-1250

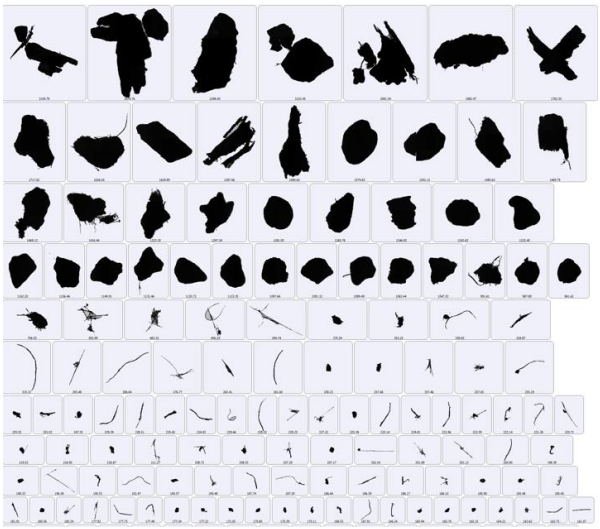

	1250-2500	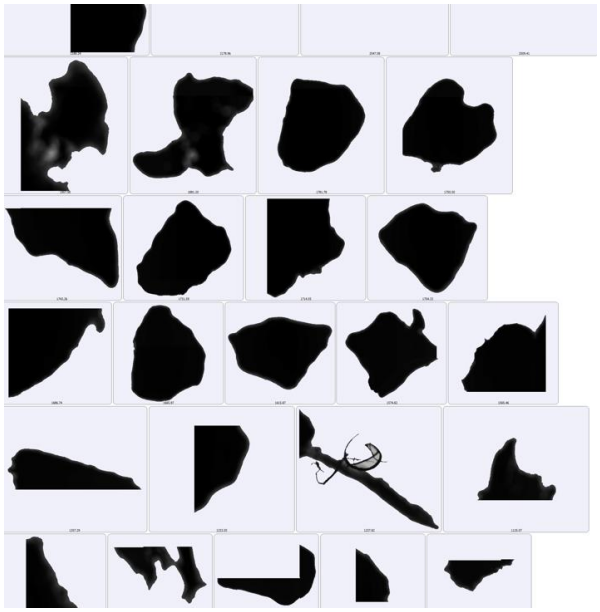
	2500-5000	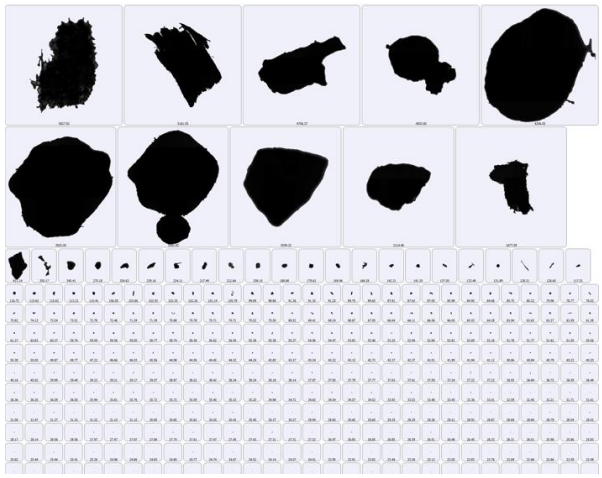
FLSC	0-500	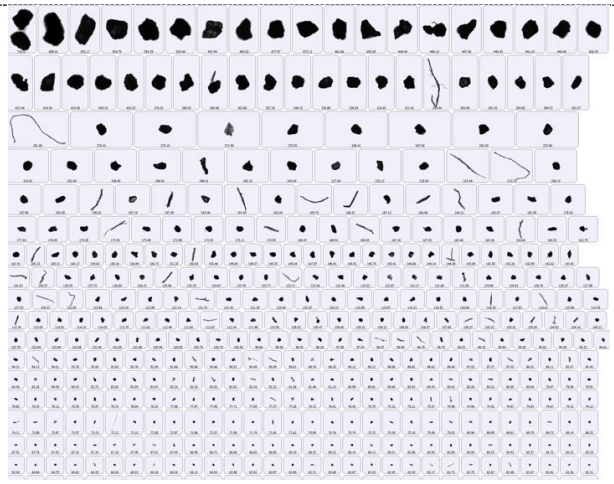

500-800

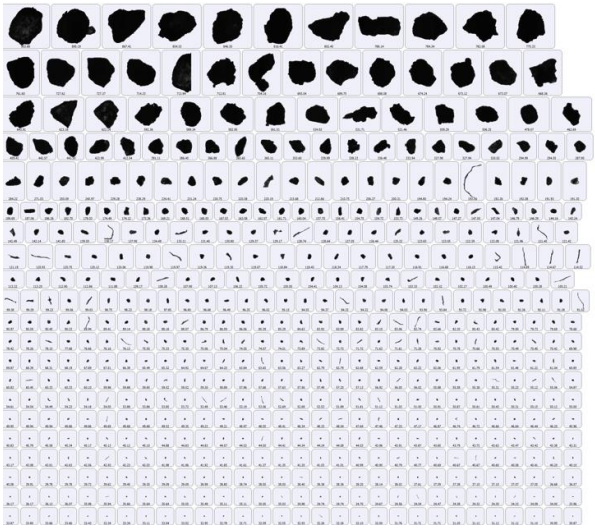

800-1250

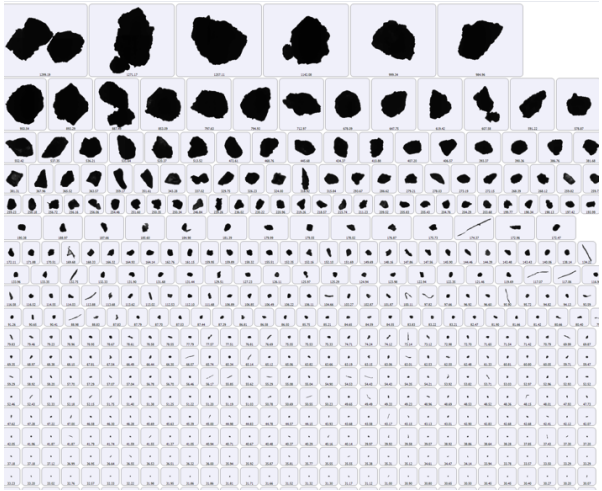

1250-2500

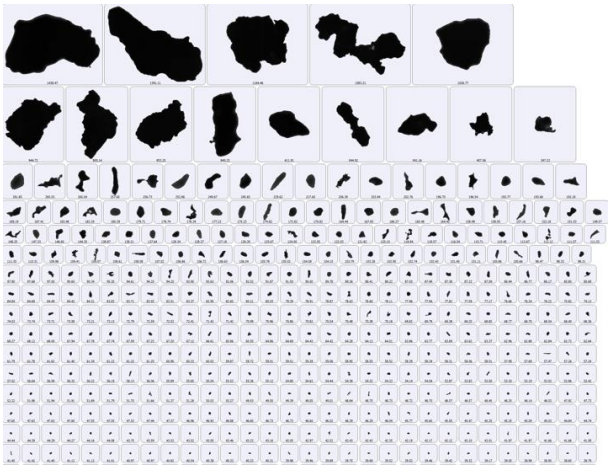

	2500-5000	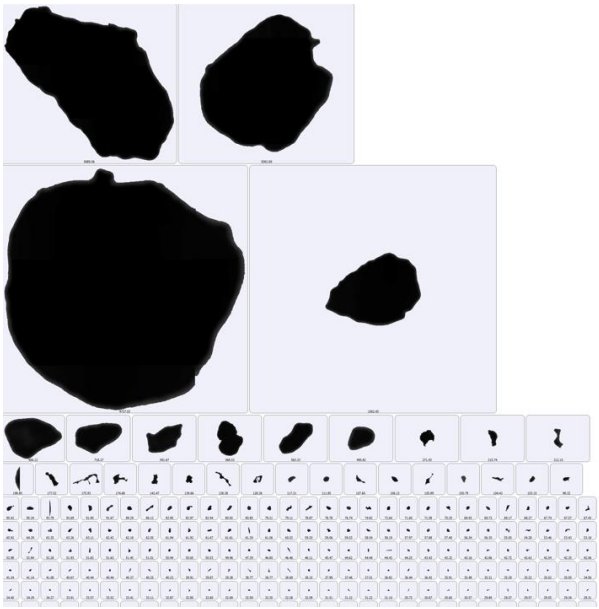
FLSM	0-500	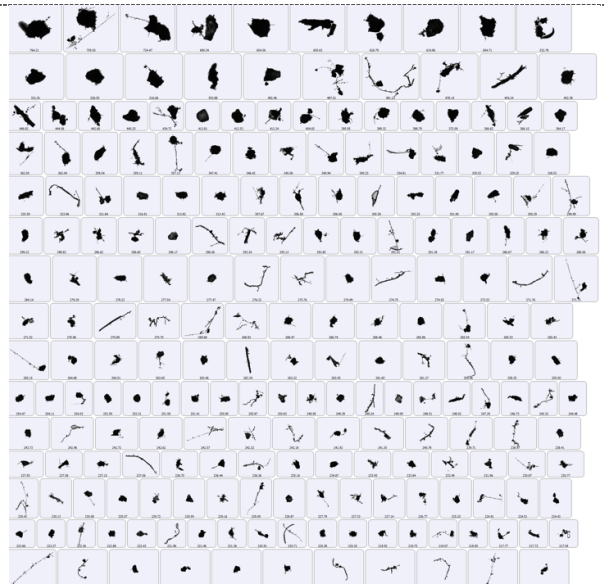

500-800

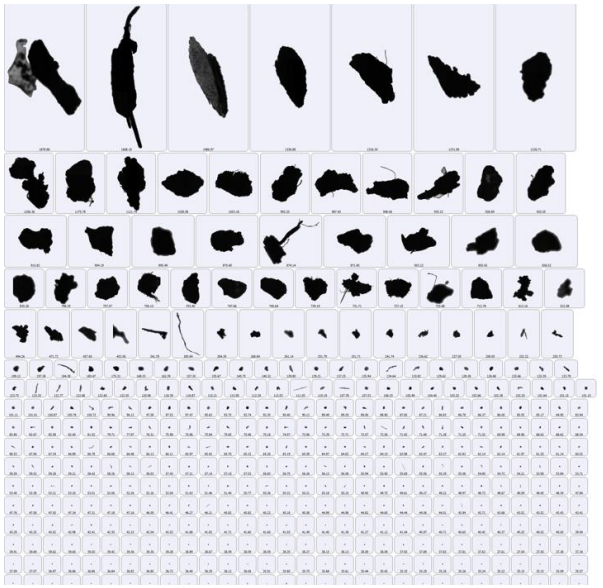

800-1250

1250-2500

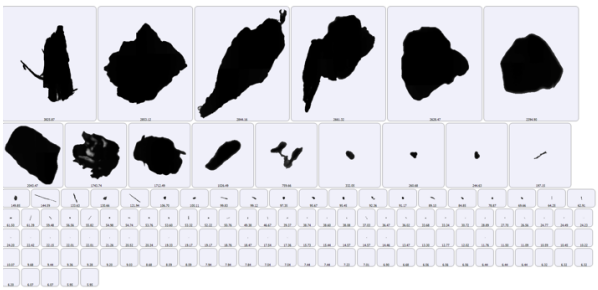

2500-5000

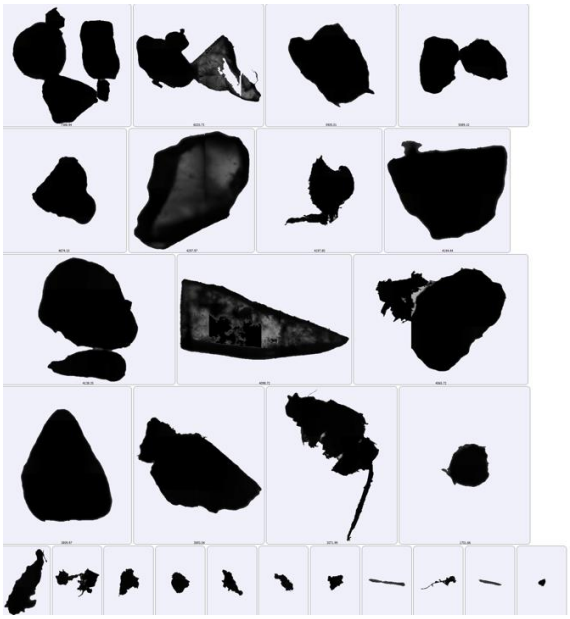

0-500

LSZM

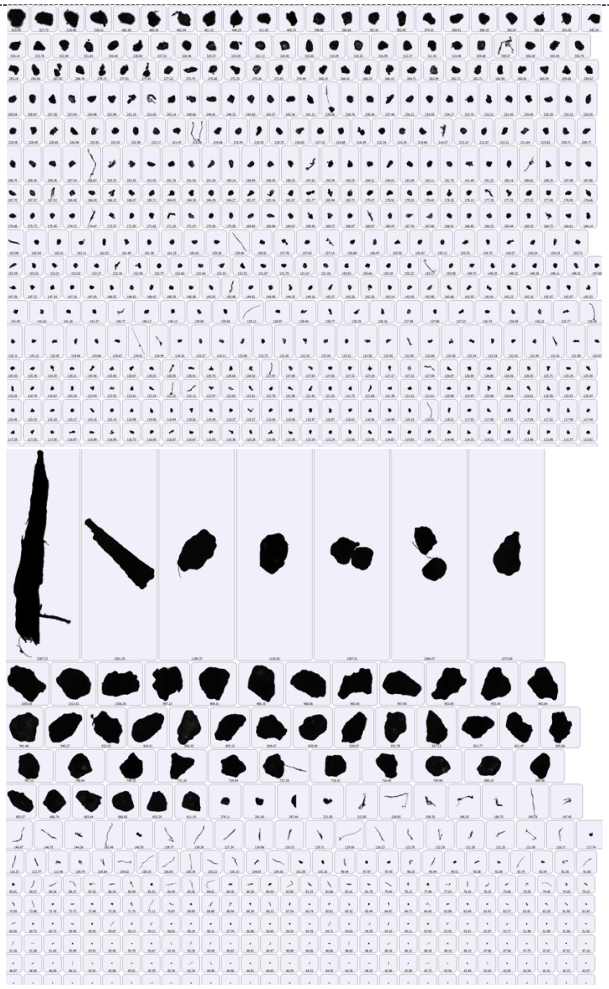

500-800

800-1250

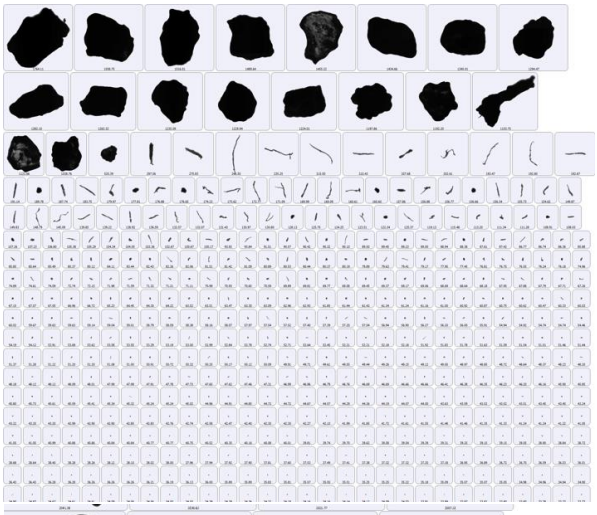

1250-2500

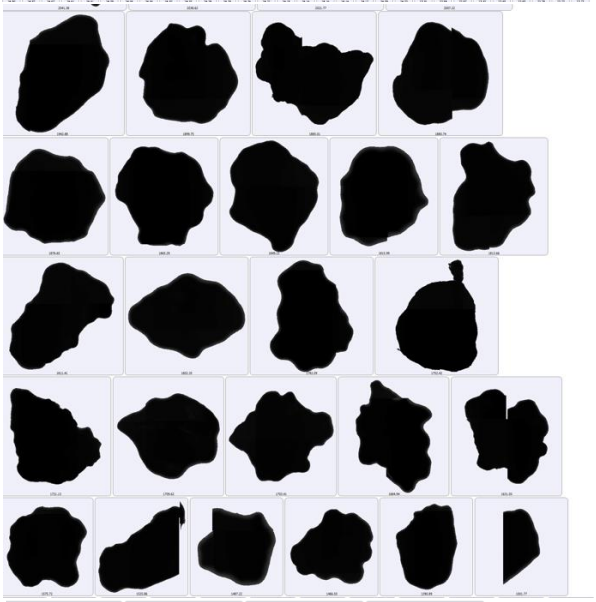

2500-5000

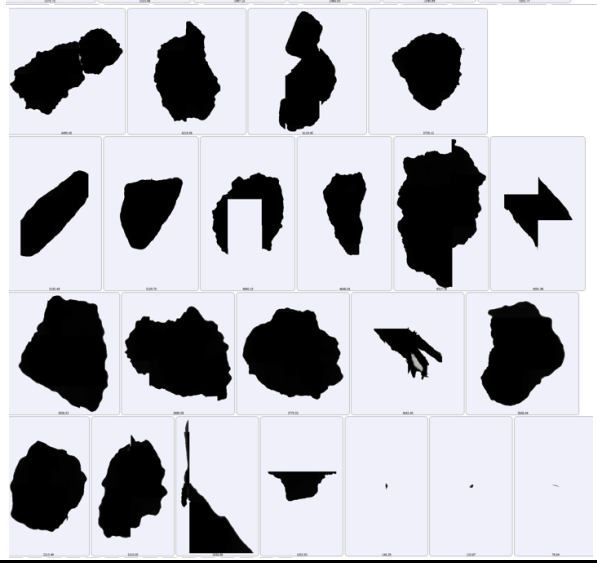

Appendix 2:

Table 11. Circularity and elongation distributions based on number and volume of the samples

Sample code	Size range (µm)	Circularity (-)	Elongation (-)
EACB	0-500 (Volume distribution)	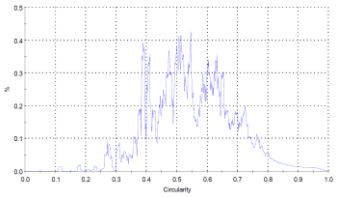	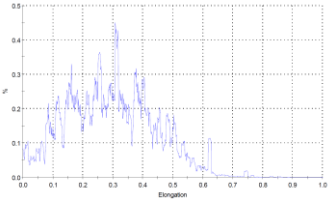
	0-500 (Number distribution)	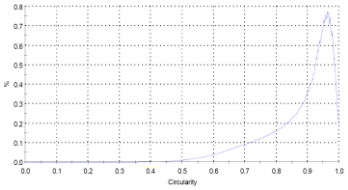	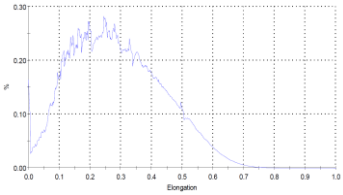
	500-800 (Volume distribution)	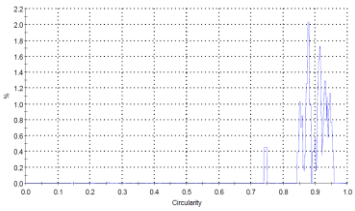	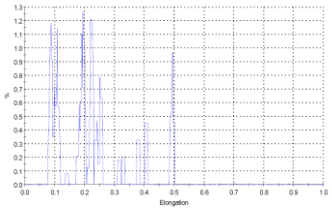
	500-800 (Number distribution)	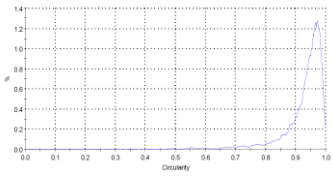	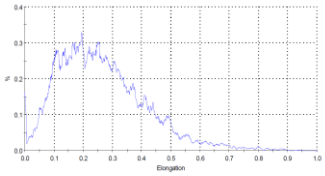

800-1250

(Volume distribution)

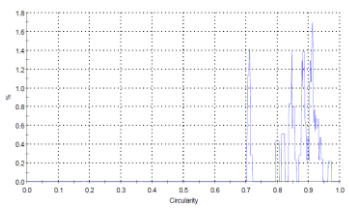
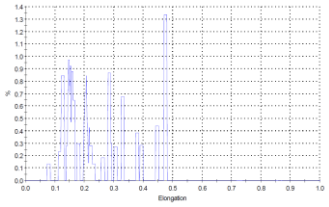

800-1250

(Number distribution)

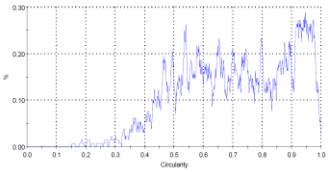
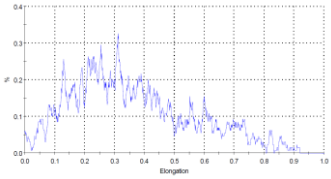

1250-2500

(Volume distribution)

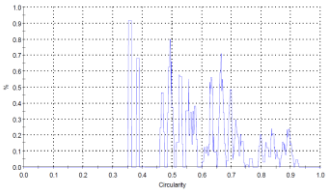
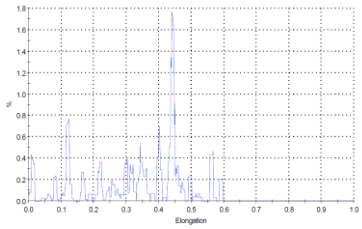

1250-2500

(Number distribution)

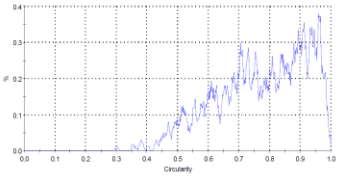
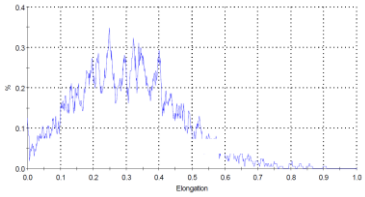

2500-5000

(Volume distribution)

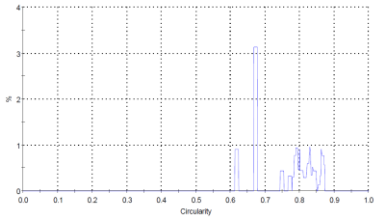
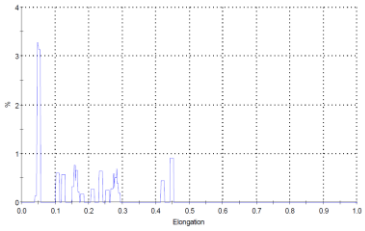

2500-5000

(Number distribution)

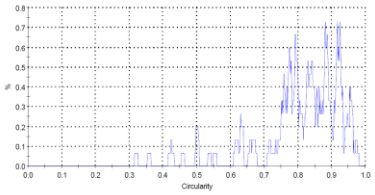

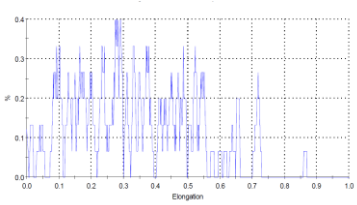

0-500

(Volume distribution)

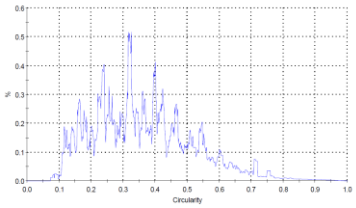

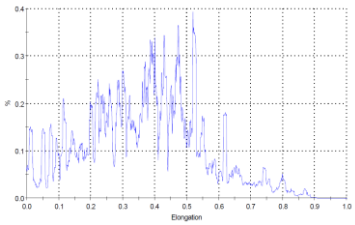

0-500

(Number distribution)

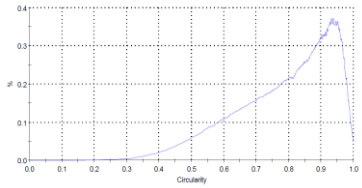

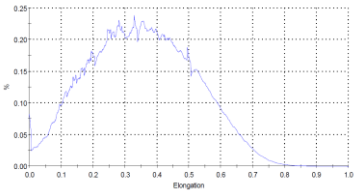

EPM

500-800

(Volume distribution)

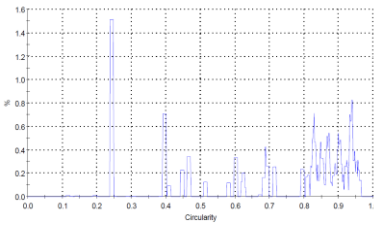

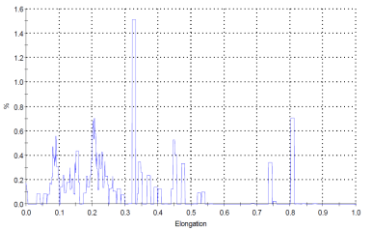

500-800

(Number distribution)

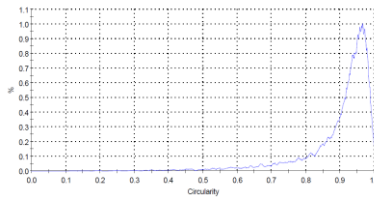

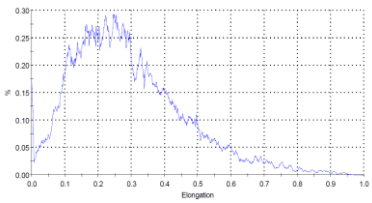

800-1250

(Volume distribution)

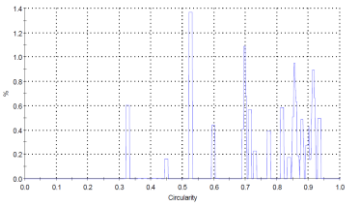

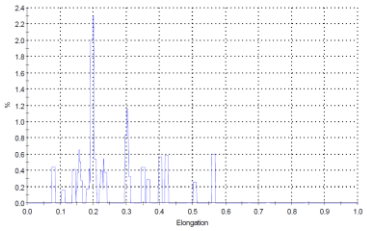

800-1250

(Number distribution)

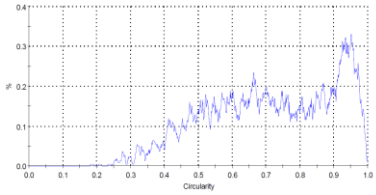

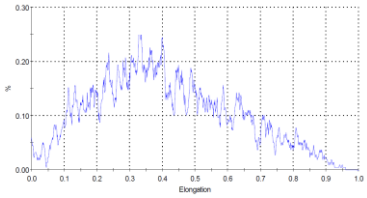

1250-2500

(Volume distribution)

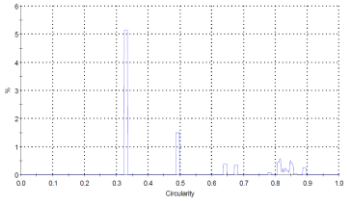

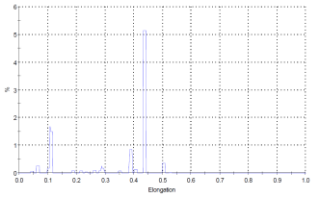

1250-2500

(Number distribution)

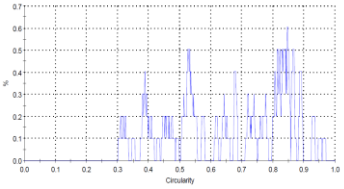

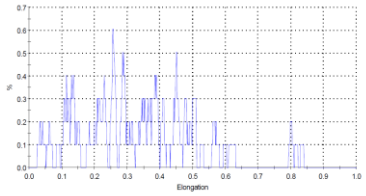

2500-5000

(Volume distribution)

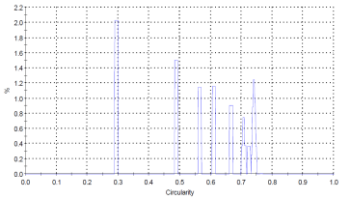

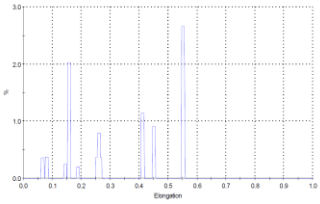

2500-5000

(Number distribution)

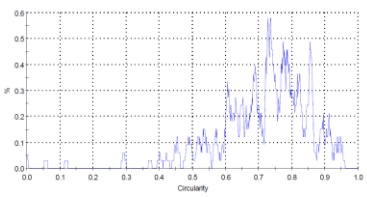

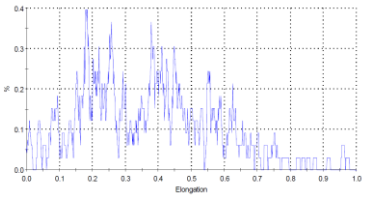

0-500

(Volume distribution)

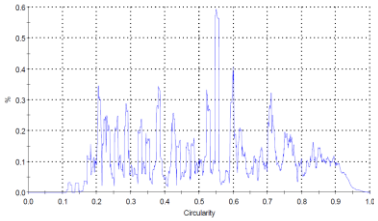

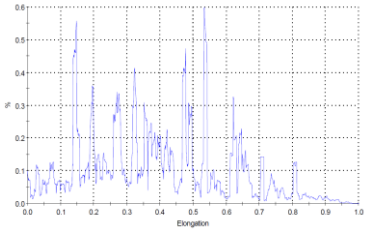

0-500

(Number distribution)

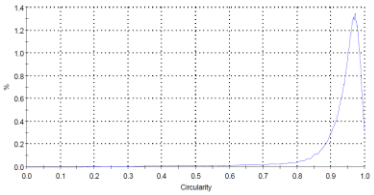

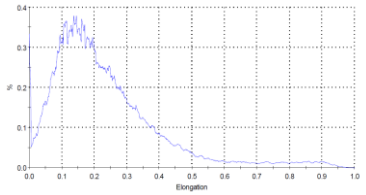

FLKM

500-800

(Volume distribution)

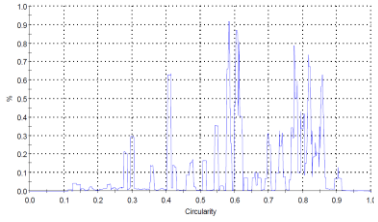

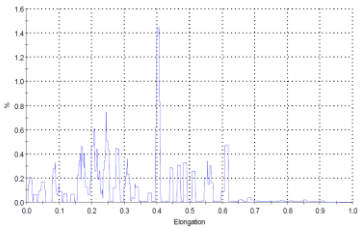

500-800

(Number distribution)

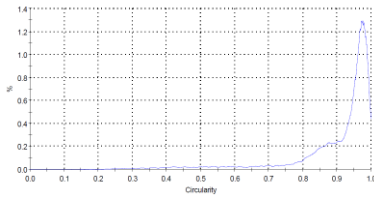

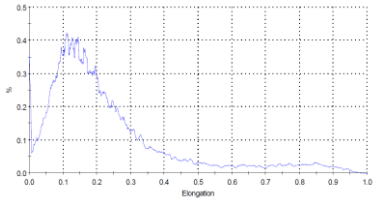

800-1250 (Volume distribution)	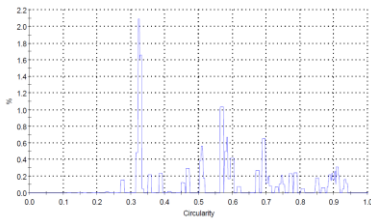	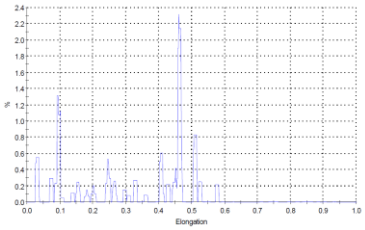
800-1250 (Number distribution)	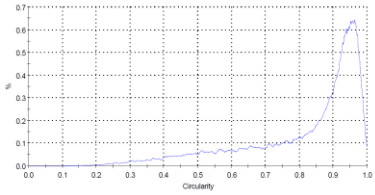	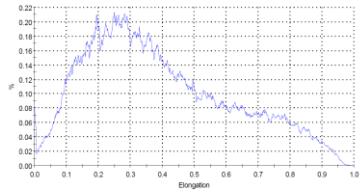
1250-2500 (Volume distribution)	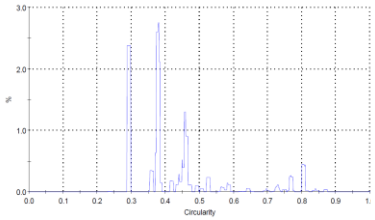	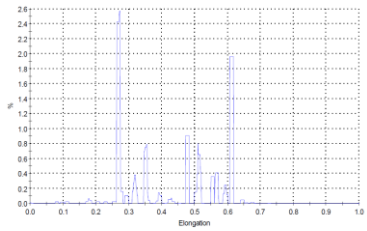
1250-2500 (Number distribution)	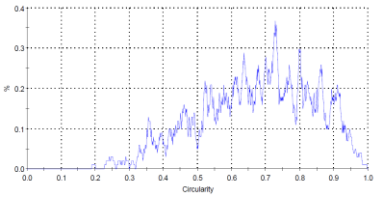	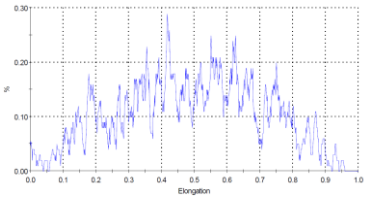
2500-5000 (Volume distribution)	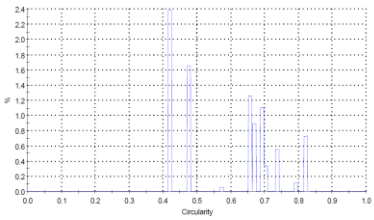	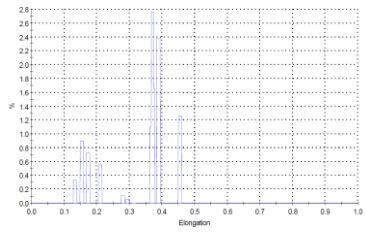

	2500-5000 (Number distribution)	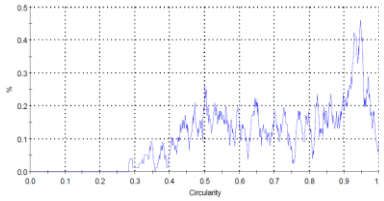	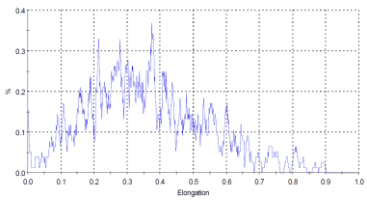
	0-500 (Volume distribution)	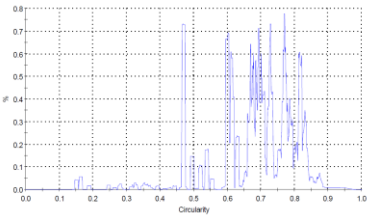	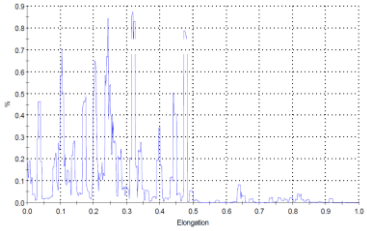
FLSC	0-500 (Number distribution)	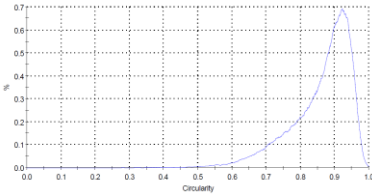	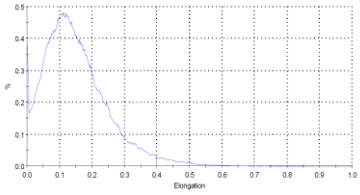
	500-800 (Volume distribution)	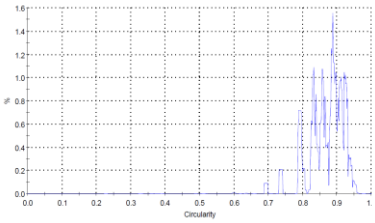	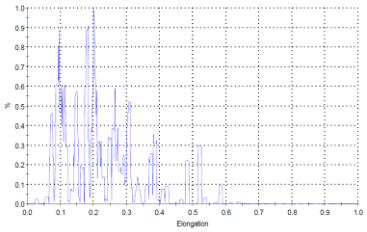
	500-800 (Number distribution)	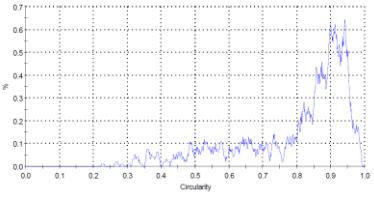	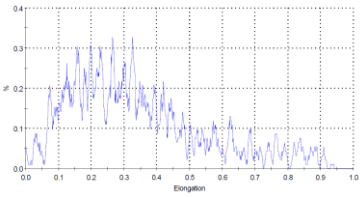

800-1250

(Volume distribution)

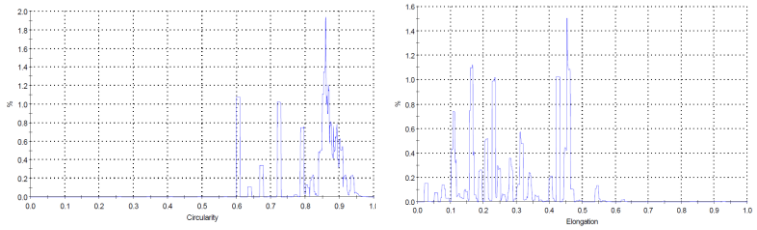

800-1250

(Number distribution)

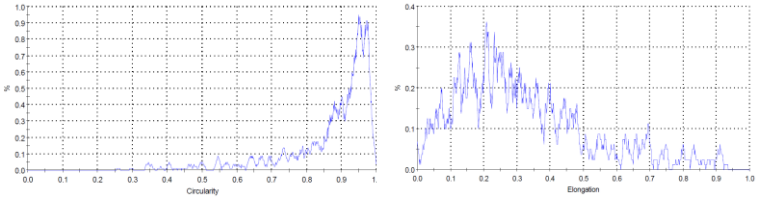

1250-2500

(Volume distribution)

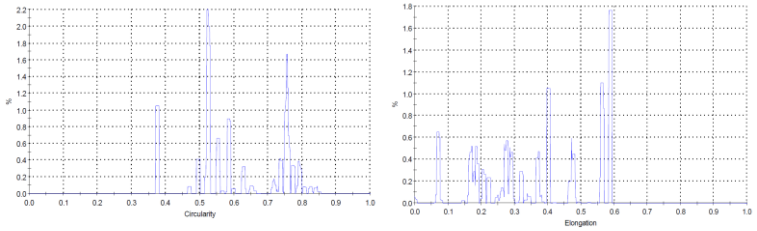

1250-2500

(Number distribution)

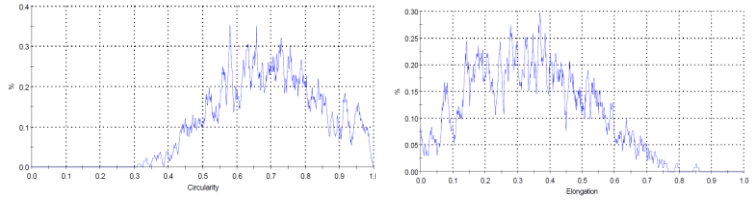

2500-5000

(Volume distribution)

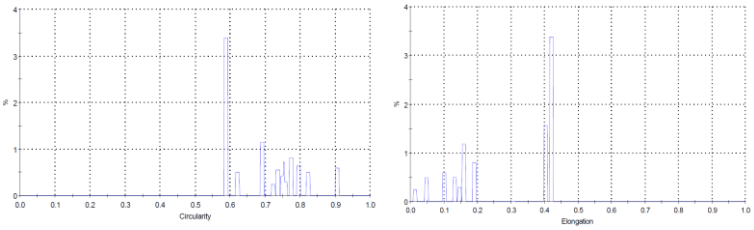

2500-5000

(Number distribution)

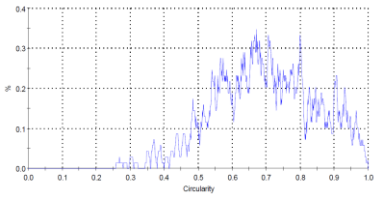

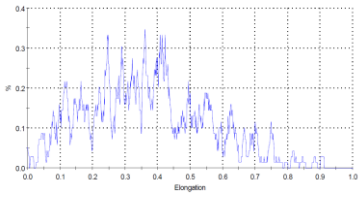

0-500

(Volume distribution)

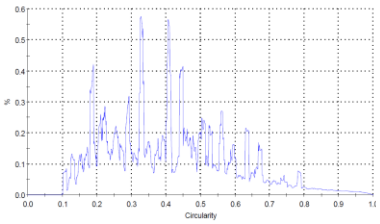

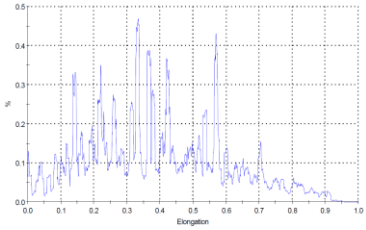

0-500

(Number distribution)

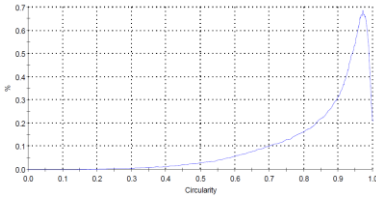

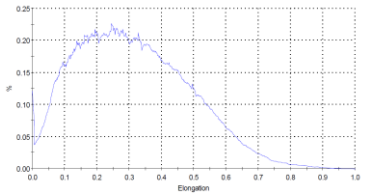

FLSM

500-800

(Volume distribution)

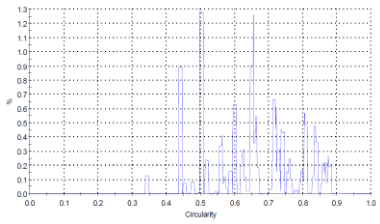

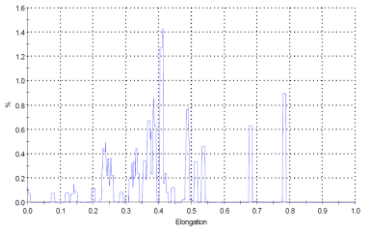

500-800

(Number distribution)

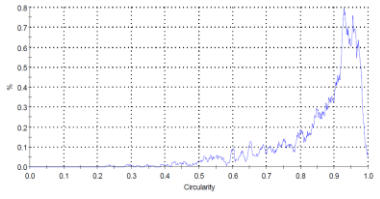

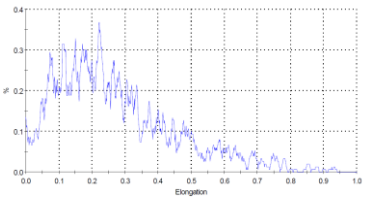

800-1250

(Volume distribution)

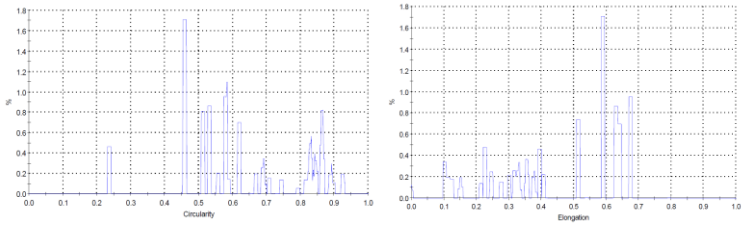

800-1250

(Number distribution)

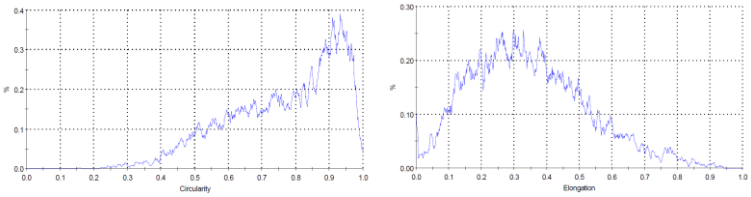

1250-2500

(Volume distribution)

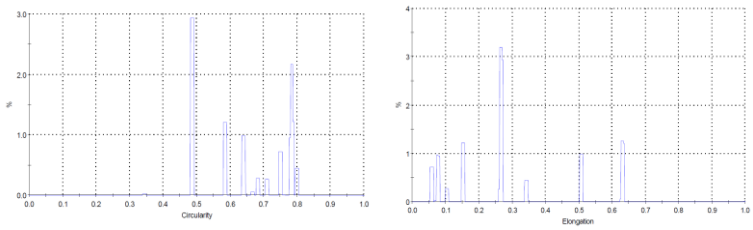

1250-2500

(Number distribution)

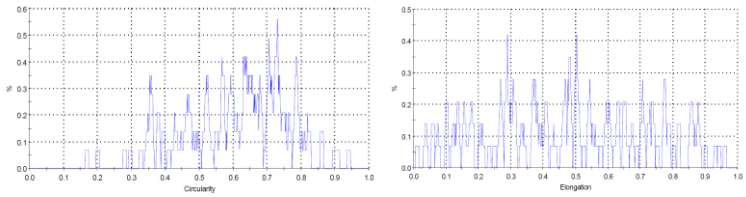

2500-5000

(Volume distribution)

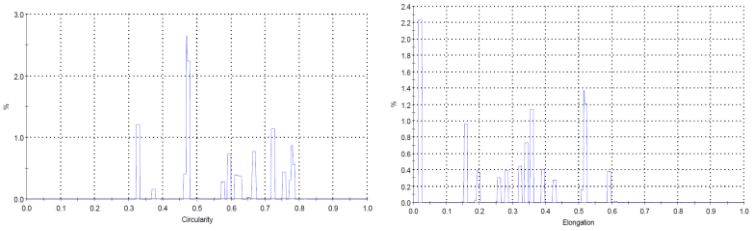

	2500-5000 (Number distribution)	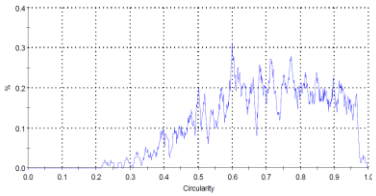	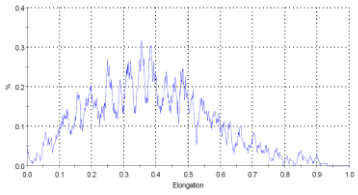
	0-500 (Volume distribution)	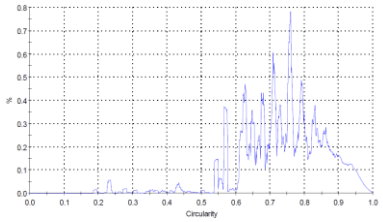	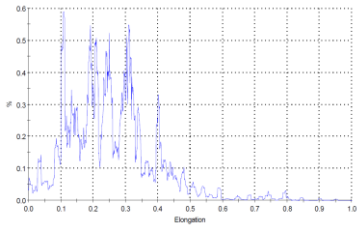
LSZM	0-500 (Number distribution)	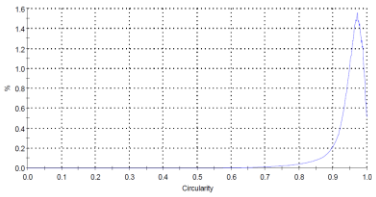	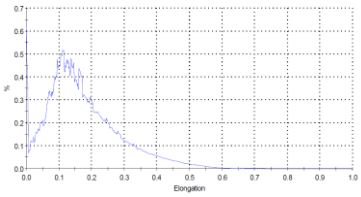
	500-800 (Volume distribution)	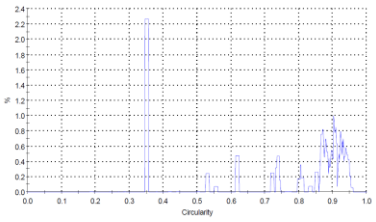	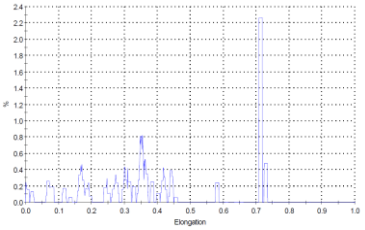
	500-800 (Number distribution)	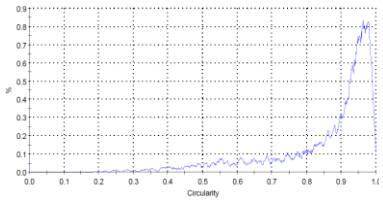	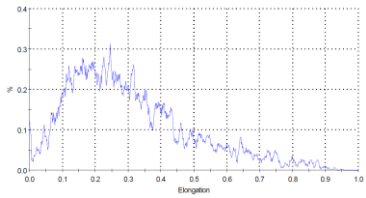

800-1250

(Volume distribution)

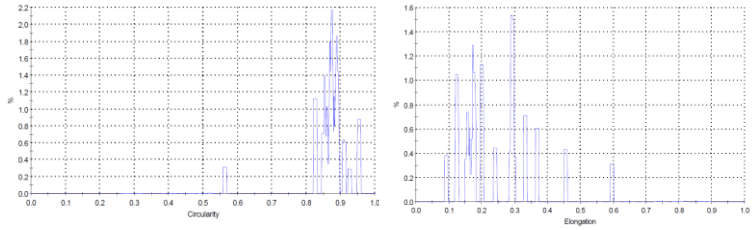

800-1250

(Number distribution)

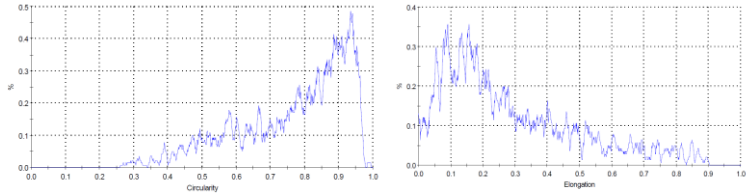

1250-2500

(Volume distribution)

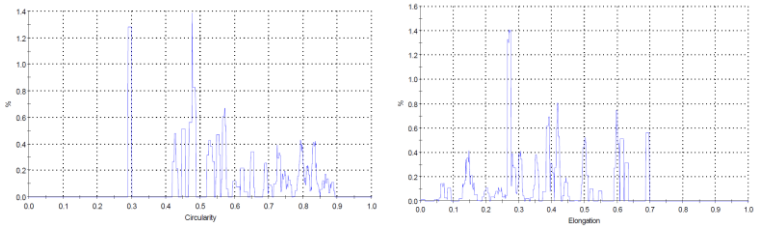

1250-2500

(Number distribution)

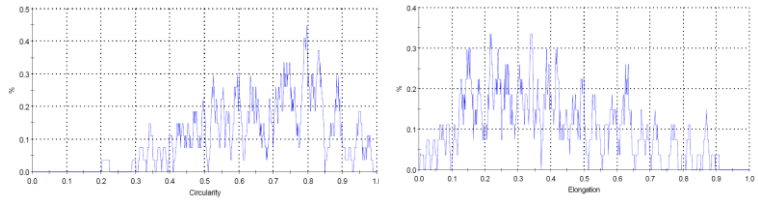

2500-5000

(Volume distribution)

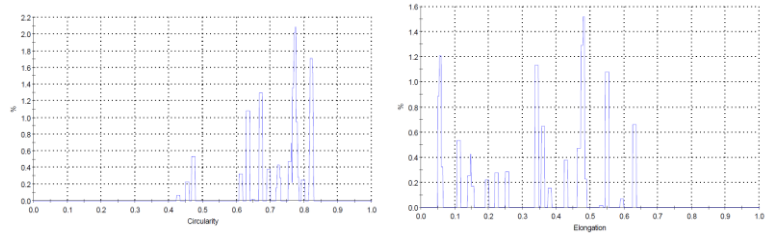

2500-5000 (Number distribution)	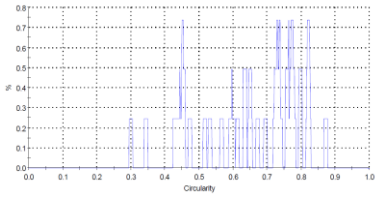	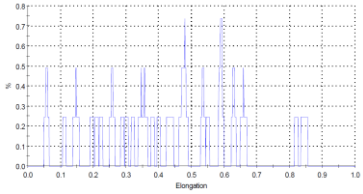

Appendix 3:

Based on the scientific principles outlined by Darcy's, Reynolds', and Ergun's equations provided in appendix 3, the particle size of the filter media can play a significant role in determining the effectiveness and flow characteristics of stormwater through the media.